JOC The Journal of Organic Chemistry

Article

pubs.acs.org/joc

DiiodoBodipy-Perylenebisimide Dyad/Triad: Preparation and Study of the Intramolecular and Intermolecular Electron/Energy Transfer

Zafar Mahmood,[†] Kejing Xu,[†] Betül Küçüköz,[‡] Xiaoneng Cui,[†] Jianzhang Zhao,*[,†] Zhijia Wang,[†] Ahmet Karatay,[‡] Halime Gul Yaglioglu,[‡] Mustafa Hayvali,*[,§] and Ayhan Elmali[‡]

[†]State Key Laboratory of Fine Chemicals, School of Chemical Engineering, Dalian University of Technology, E-208 West Campus, 2 Ling-Gong Road, Dalian 116024, People's Republic of China

[‡]Department of Engineering Physics, Faculty of Engineering, and [§]Department of Chemistry, Faculty of Science, Ankara University, 06100 Beşevler, Ankara, Turkey

Supporting Information

ABSTRACT: 2,6-diiodoBodipy-perylenebisimide (PBI) dyad and triad were prepared, with the iodoBodipy moiety as the singlet/triplet energy donor and the PBI moiety as the singlet/triplet energy acceptor. IodoBodipy undergoes intersystem crossing (ISC), but PBI is devoid of ISC, and a competition of intramolecular resonance energy transfer (RET) with ISC of the diiodoBodipy moiety is established. The photophysical properties of the compounds were studied with steady-state and femtosecond/nanosecond transient absorption and emission spectroscopy. RET and photoinduced electron transfer (PET) were confirmed. The production of the triplet state is high for the iodinated dyad and the triad (singlet oxygen quantum yield Φ_Δ = 80%). The Gibbs free energy changes of the electron transfer (ΔG_{CS}) and the energy level of the charge transfer state (CTS) were analyzed. With nanosecond transient absorption spectroscopy, we confirmed that the triplet state is localized on the PBI moiety in the iodinated dyad and the triad. An exceptionally long lived triplet excited state was observed (τ_T = 150 μs) for PBI. With the uniodinated reference dyad and triad, we demonstrated that the triplet state localized on the PBI moiety in the iodinated dyad and triad is not produced by charge recombination. These information are useful for the design and study of the fundamental photochemistry of multichromophore organic triplet photosensitizers.

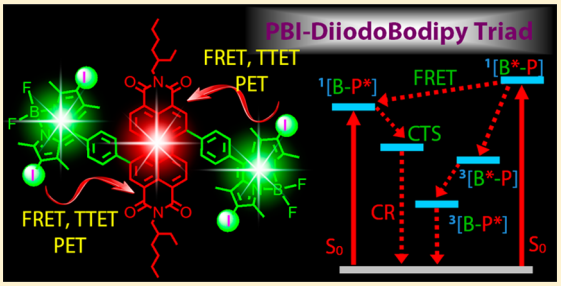

1. INTRODUCTION

Recently triplet photosensitizers have attracted much attention,[1−7] due to the applications of these versatile materials in photodynamic therapy,[4] photocatalyses such as photocatalytic hydrogen (H_2) production,[8] photoredox catalytic synthetic organic reactions,[9] photoinitiated polymerization,[10] and more recently triplet−triplet annihilation assisted upconversion.[6,11−15] Conventional triplet photosensitizers are limited to porphyrin derivatives (including Zn(II), Pt(II), or Pd(II) complexes)[16−19] and halogenated xanthane dyes, such as Rose Bangle or Methylene blue,[6,20] as well as some ketone compounds, such as benzophenone, diacetyl, ketocoumarin, etc.[6,21,22] Transition-metal complexes such as Pt(II), Ir(III), and Ru(II) complexes have also been used as triplet photosensitizers.[6,23] However, these compounds suffer from drawbacks such as difficulties in preparation/purification, loss of ISC upon derivatization (although in some cases careful functionalization may leave ISC intact), and weak visible light absorption.[6]

New triplet photosensitizers have been developed: for example, the bromo- or iodo-Bodipys and the heavy-atom-free Bodipy dimers.[1,4,5,24,25] These compounds show strong absorption of visible light and long-lived triplet excited states and have been used in photodynamic therapy (PDT) studies.[4,5,24] Moreover, transition-metal complexes with strong absorption of visible light and long-lived triplet excited states have also been developed and have been studied for triplet−triplet annihilation (TTA) upconversion.[6,15,26−29]

However, all these new triplet photosensitizers suffer a common drawback: that is, the molecular structure is based on a single chromophore protocol and, as a result, these compounds show only one major absorption band in the visible spectral region. Thus, these compounds are inefficient for harvesting the photoexcitation energy from a *broad-band* light source, such as solar light.[6] Therefore, it is important to prepare a broad-band visible-light-absorbing triplet photosensitizer.[30] Inspired by the popular method of fluorescence resonance energy transfer (FRET),[7a,3b,31−34] we proposed to prepare triplet photosensitizers on the basis of the RET of chromophore dyads or triads to attain broad-band visible light absorption. Following this method, we have prepared broad-band visible-light-absorbing triplet photosensitizers based on Bodipy dyads or triads.[35,36] Previously Bodipy dyads showing broad-band visible light absorption were studied from the perspective of molecular logic gates.[30,37] However, the fundamental photophysical properties for these multichromophore triplet photosensitizers

Received: December 22, 2014
Published: February 24, 2015

DOI: 10.1021/jo502899p
J. Org. Chem. 2015, 80, 3036−3049

Scheme 1. Synthesis of the Triplet Photosensitizers B-1 and B-2 and the Reference Compounds L-1, L-2, and L-3[a]

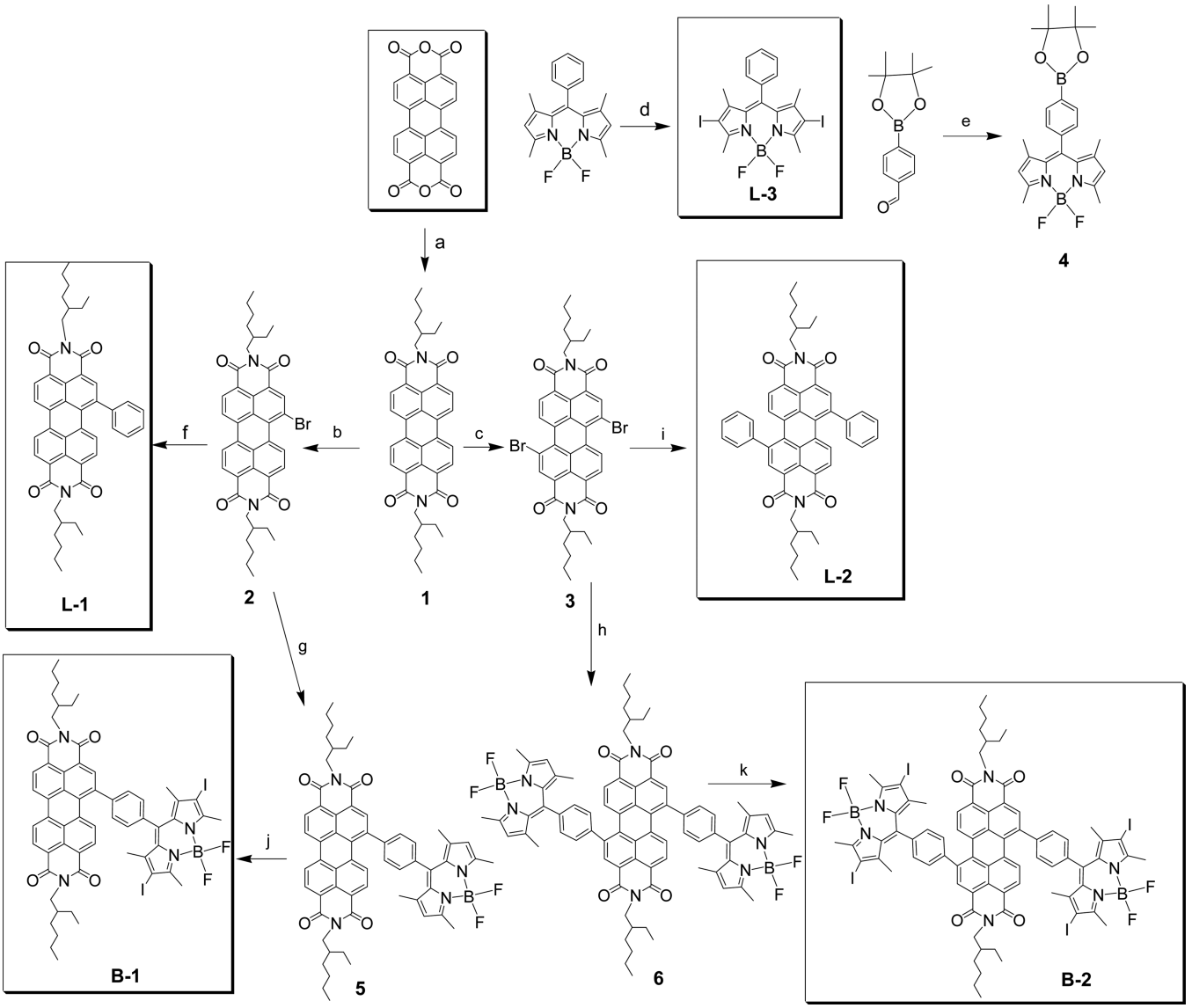

[a]Legend: (a) 2-ethylhexylamine, imidazole, refluxed at 160 °C for 8 h, under Ar; (b) Br_2, $CHCl_3$, stirred at room temperature for 48 h under Ar; (c) Br_2, $CHCl_3$, stirred at 60 °C for 48 h under Ar; (d) 4 equiv of *N*-iodosuccinimide (NIS), DCM, stirred for 30 min at room temperature; (e) DDQ, TFA, stirred overnight at room temperature under Ar, and then $BF_3{\cdot}Et_2O$, Et_3N, stirred for 2 h under ice-cold conditions; (f) phenylboronic acid, K_2CO_3, $Pd(PPh_3)_4$, $PhCH_3/C_2H_5OH/H_2O$ (4/2/1, v/v), refluxed at 90 °C for 8 h, under Ar; (g) K_2CO_3, $Pd(PPh_3)_4$, $PhCH_3/C_2H_5OH/H_2O$ (4/2/1, v/v), reflux 90 °C for 8 h, under Ar; (h) K_2CO_3, $Pd(PPh_3)_4$, $PhCH_3/C_2H_5OH/H_2O$ (4/2/1, v/v), refluxed at 90 °C for 8 h under Ar; (i) phenylboronic acid, K_2CO_3, $Pd(PPh_3)_4$, $PhCH_3/C_2H_5OH/H_2O$ (4/2/1, v/v), refluxed at 90 °C for 8 h, under Ar; (j) excess NIS, stirred for 5 h at room temperature; (k) excess NIS, stirred for a long time at 30 °C.

have still not been fully elucidated, such as the competition of resonance energy transfer (RET) and intersystem crossing (ISC); these processes have not yet been studied with femtosecond or nanosecond transient absorption spectroscopy for multichromophore organic triplet photosensitizers. Previously it was proposed that the ISC of intramolecular singlet energy donors was inhibited by intramolecular RET.[30,37] However the rich photophysical properties of multichromophore dyads/triads have yet to be fully studied. Visible-light-harvesting dyads or triads with intramolecular energy transfer and production of triplet excited states were reported, but none of these compounds were designed to be with competitive RET and ISC processes.[38−42] Establishment of such a competition between ISC and FRET requires that the singlet energy donor is also a spin converter. Such dyads/triads have never been reported.[43]

In order to take an in-depth look into the uncharted photophysical processes involved in the multichromophore organic triplet photosensitizers, herein we have prepared an iodoBodipy-perylenebisimide (PBI) dyad and triad (**B-1** and **B-2**, Scheme 1). For these compounds, both the PBI and the Bodipy moiety show strong absorption of visible light;[44−49] the singlet state energy levels ensure RET. The singlet energy donor iodoBodipy shows ISC capability, whereas the singlet energy acceptor PBI is devoid of ISC. Moreover, the ISC of the diiodoBodipy will be competed by the FRET, with which the production of the triplet excited state is presumably inhibited. The photophysical properties of the dyad and triad were studied

DOI: 10.1021/jo502899p
J. Org. Chem. 2015, 80, 3036−3049

with steady-state and femto-/nanosecond transient absorption and emission spectroscopy, as well as electrochemical characterization. Photoinduced electron transfer (PET) was confirmed for the dyad and triad. We found that the ISC of the iodoBodipy part is unable to be completely inhibited by the RET to PBI, and surprisingly the dyad and triad show high singlet oxygen quantum yields (Φ_Δ). The charge-separated state (CST) lies at a higher energy level than the triplet excited state.

Nanosecond transient absorption spectroscopy indicated that the triplet excited state of the dyad and the triad is exclusively localized on the PBI moiety, and the triplet state lifetime of the PBI moiety (150 μs) is much longer than that previously observed. With uniodinated dyad and triad we confirmed that the production of the triplet state in the dyad and triad is not due to charge recombination. These studies are useful for the design of new broad-band visible-light-absorbing organic triplet photosensitizers and study of the photophysical properties of these organic chromophores.

2. RESULTS AND DISCUSSION

2.1. Design and Synthesis of the Compounds. 2,6-diiodoBodipy was selected as the singlet energy donor/spin converter, due to its strong absorption of visible light and efficient ISC.[4,50] PBI was used as the singlet energy acceptor.[38] On the basis of the fluorescence emission of the Bodipy and iodoBodipy and the absorption spectra of PBI, we envisage that RET will occur with Bodipy as an energy donor and PBI as an energy acceptor.[51,52] As a result, ISC of iodo-Bodipy will compete with RET. Note that the PBI moiety is devoid of ISC capability. Moreover, the T_1 state energy level of the PBI moiety (1.2 eV) is lower than that of Bodipy (ca. 1.7 eV).[38,53,54] Thus, the triplet state of the dyad or triad, if populated by any mechanism, will be located on the PBI moiety, not the Bodipy moiety.[55,56] To the best of our knowledge, PBI-Bodipy molecular dyads or triads have never been used for studies of the triplet state manifold. The only example of a Bodipy-PBI assembly (a dendrimer) was used for a singlet energy transfer study: i.e., fluorescence-related studies.[52] All of the compounds were synthesized by routine procedures (Scheme 1).

2.2. UV–Vis Absorption and Fluorescence Emission Spectra. The UV–vis absorption spectra of the compounds were studied (Figure 1). For **L-1**, moderate absorption bands at

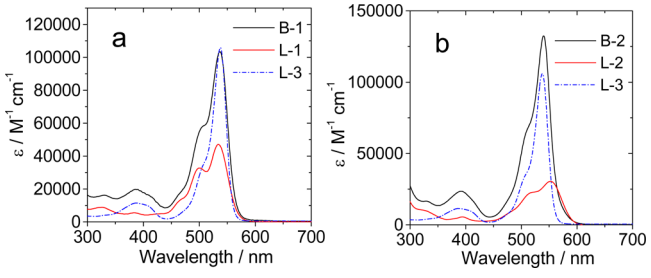

Figure 1. UV–vis absorption spectra of (a) **B-1**, **L-1**, and **L-3** and (b) **B-2**, **L-2**, and **L-3**. Conditions: c = 1.0 × 10^{-5} M in toluene; 20 °C.

500 nm (ε = 32000 M^{-1} cm^{-1}) and 535 nm (ε = 47000 M^{-1} cm^{-1}) were observed. For **L-3**, a strong absorption at 538 nm was observed (ε = 106000 M^{-1} cm^{-1}), which is the signature absorption of the Bodipy chromophore.[57,58] The absorption spectrum of **B-1** is not the sum of **L-1** and **L-3** with regard to the molar absorption coefficients, although the absorption wavelengths are similar. Similar results were observed for **B-2**. These results may be due to the close proximity of the Bodipy and PBI chromophores.[52] The UV–vis absorptions of the compounds in other solvents were also studied (see the Supporting Information, Figures S31–S33).

In order to study the RET process, the fluorescence emissions of the singlet energy donor **L-3** and that of dyad **B-1** were compared (Figure 2a). With optically matched solutions (i.e., the

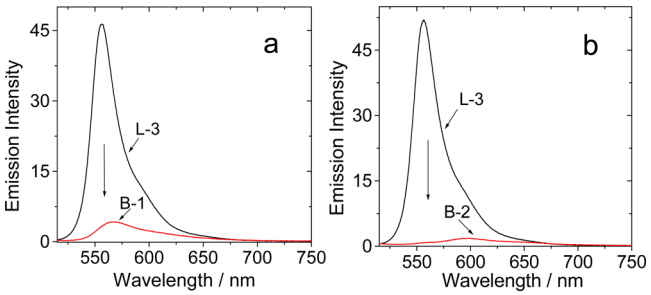

Figure 2. Quenching of the fluorescence of the energy donor (iodoBodipy) in dyad **B-1** and triad **B-2**: (a) Fluorescence spectra of **B-1** and **L-3**, λ_{ex} 508 nm; (b) fluorescence spectra of **B-2** and **L-3**, λ_{ex} 480 nm. In (a) and (b) optically matched solutions were used (i.e., the absorbance of the two samples at the excitation wavelength are same). Conditions: c = ca. 1.0 × 10^{-5} M in toluene (slight variation of the concentration is necessary to prepare optically matched solutions); 20 °C.

solutions show the same optical density, or absorbance, at an excitation wavelength of 508 nm), the two compounds give drastically different emission intensities: i.e., the emission of **L-3** is substantially quenched in **B-1**. Similar results were observed for the comparison of **L-3** and **B-2** (Figure 2b; the emission of **B-2** is attributed to the emission of the PBI moiety). The quenching of the emission of **L-3** in **B-1** is most probably due to intramolecular energy transfer,[59−61] although electron transfer cannot be excluded. Femtosecond transient absorption spectroscopy indicated that the quenching is due to the FRET effect (see below). Similar quenching effects were also observed in other solvents such as dichloromethane and acetonitrile (see the Supporting Information, Figure S36).

The PET effects in **B-1** and **B-2** were studied by comparison of the fluorescence emission of the energy *acceptor* in the dyad/triad, i.e. the PBI moiety **L-1**/**L-2**, with that of **B-1**/**B-2** (Figure 3a).[32,47,59] Quenching of the energy acceptor emission in the

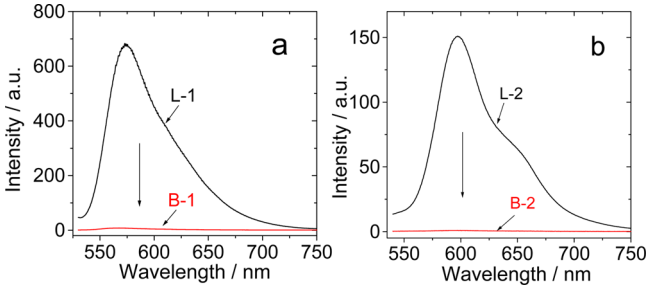

Figure 3. Confirmation of the photoinduced electron transfer by fluorescence quenching of the energy acceptor in **B-1** and **B-2**: (a) fluorescence spectra of **B-1** and **L-1** in toluene, λ_{ex} = 515 nm; (b) fluorescence spectra of **B-2** and **L-2** in toluene, λ_{ex} = 460 nm. In (a) and (b), optically matched solutions were used. Conditions: c = ca. 1.0 × 10^{-5} M in toluene (slight variation of the concentration is necessary to prepare optically matched solutions); 20 °C.

DOI: 10.1021/jo502899p
J. Org. Chem. 2015, 80, 3036−3049

Table 1. Photophysical Properties of the Compounds

	λ_{abs} [a]	ε [b]	λ_{em}	Φ_F [c]	τ_T [d]	τ_F [e]	Φ_Δ [f]
B-1	537	1.03	566	0.18	150	0.96	0.80
B-2	541	1.32	597	0.05	148	0.84	0.78
5	504/534	1.09/0.37	514/549	1.04	*g*	2.8/3.2	*g*
6	504/552	1.73/0.25	520/595	0.16	*g*	3.3/4.5	*g*
L-1	534	0.47	574	42.4	*g*	5.96	0.08
L-2	552	0.31	597	50.5	*g*	7.30	*g*
L-3	538	1.06	554	2.7[h]	90	0.29	0.83[h]
Bodipy	504	1.09	514	72.0[h]	*g*	3.86	*g*

[a]In toluene (1.0×10^{-5} M), in nm. [b]Molar absorption coefficient, in 10^5 M^{-1} cm^{-1}. [c]Fluorescence quantum yield, in percent. [d]Triplet excited state lifetimes, in μs; measured by nanosecond transient absorption in deaerated solutions. [e]Luminescence lifetimes, in ns. [f]Singlet oxygen quantum yield (Φ_Δ) with diiodoBodipy as a standard (Φ_Δ = 0.83 in DCM) at λ_{ex} 531 nm. [g]Not applicable. [h]Literature value.

dyad or triad indicates a PET effect. With an optically matched solution at the excitation wavelength (λ_{ex} = 515 nm), the emission of **B-1** is much weaker in comparison with that of **L-1**. Similar results were observed for the comparison of **L-2**/**B-2** (Figure 3b). The fluorescence quantum yields (Φ_F) of **L-1** and **L-2** were determined as being 42.4% and 50.5%, respectively. The fluorescence quantum yields decreased to less than 1% in **B-1** and **B-2** (Table 1). The quenching of the acceptor emission is attributed to intramolecular electron transfer.[59] A similar quenching effect was also observed in other solvents such as dichloromethane and acetonitrile (Figures S38 and S39, Supporting Information). In a previously reported PBI-Bodipy assembly, such electron-transfer-induced quenching of the acceptor fluorescence was not studied.[52]

The intramolecular electron transfer rate constants were calculated with eq 1 based on the fluorescence lifetimes of **L-1** and **L-2**, and the quenched fluorescence quantum yields of **L-1** and **L-2** in **B-1** and **B-2**, respectively.[59]

$$k_{CS}^{intra} = \frac{\left[\frac{\Phi_{PL}(\textbf{B-1 or B-2})}{\Phi_{PL}}\right]}{\tau(\textbf{L-1 or L-2})} \quad (1)$$

The photoinduced intramolecular electron transfer rate constants of **B-1** and **B-2** in toluene were calculated as k_{CS}^{intra} = 3.8×10^{10} and 1.4×10^{11} s^{-1}, respectively. These values are close to the electron transfer rate constant observed in calix[4]arene-PBI dyad (k_{CS}^{intra} = 4.0×10^{10} s^{-1} in toluene; k_{CS}^{intra} is solvent-dependent).[62]

To further confirm the intramolecular electron transfer in **B-1**, the fluorescence of **B-1** in solvents with different polarities was studied (Figure 4). The electron transfer induced fluorescence quenching will be more significant in polar solvents.[32] The emission intensity of **B-1** in a nonpolar solvent such as toluene is stronger than that in polar solvents, such as dichloromethane and acetonitrile (Figure 4a). For the components of dyad **B-1**, i.e. **L-1** and **L-3**, however, fluorescence emission intensity is much less dependent on the solvent polarity (Figure 4b,c). These results confirm the photoinduced electron transfer in **B-1**, which is more significant in polar solvents.[32] Similar results were observed for **B-2** and the reference compounds (Figure S40, Supporting Information). The photophysical properties of the compounds are summarized in Table 1.

2.3. Redox Properties: Cyclic Voltammogram of the Compounds. The electrochemical properties of the dyad **B-1** and the triad **B-2** were studied with cyclic voltammograms (CV; Figures 5 and 6). These electrochemical data can be used for evaluation of the free energy changes of the photoinduced intramolecular electron transfer, as well as the energy level of the

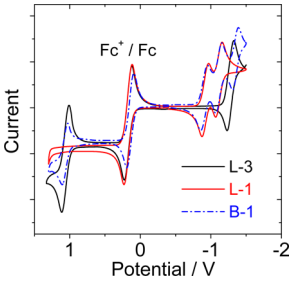

Figure 5. Cyclic voltammograms of **L-3**, **B-1**, and **L-1**. Ferrocene (Fc) was used as internal reference ($E_{1/2}$ = +0.64 V (Fc^+/Fc) vs standard hydrogen electrode). Conditions: in deaerated CH_2Cl_2 solutions containing 0.5 mM photosensitizers with the ferrocene, 0.10 M Bu_4NPF_6 as supporting electrolyte, $Ag/AgNO_3$ reference electrode, scan rate 50 mV/s, 20 °C.

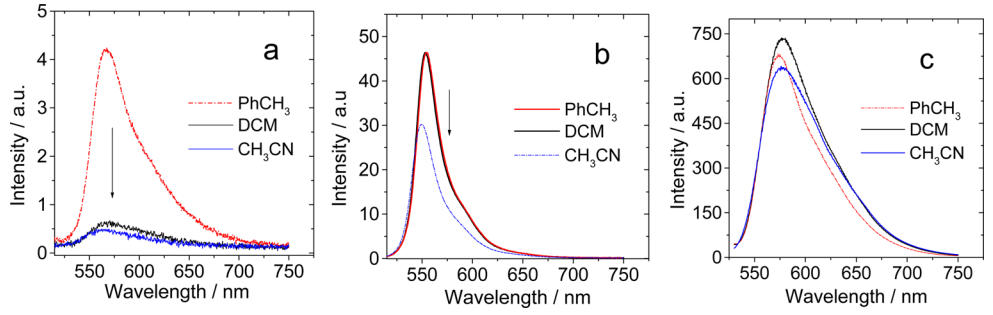

Figure 4. Fluorescence emission spectra: (a) **B-1** (λ_{ex} 508 nm); (b) **L-3** (λ_{ex} 508 nm); (c) **L-1** (λ_{ex} 515 nm). Optically matched solutions were used. Conditions: 20 °C.

DOI: 10.1021/jo502899p
J. Org. Chem. 2015, 80, 3036−3049

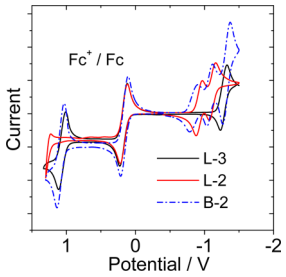

Figure 6. Cyclic voltammograms of **L-3**, **L-2**, and **B-2**. Ferrocene (Fc) was used as internal reference ($E_{1/2}$ = +0.64 V (Fc^+/Fc) vs standard hydrogen electrode). Conditions: in deaerated CH_2Cl_2 solutions containing 0.5 mM photosensitizers with the ferrocene, 0.10 M Bu_4NPF_6 as supporting electrolyte, $Ag/AgNO_3$ reference electrode, scan rate 50 mV/s, 20 °C.

charge transfer state (CTS),[64] which are useful for explanation of the photophysical processes of **B-1** and **B-2**. A reversible oxidation wave at +1.52 V was observed for **L-3** (Figure 5). Conversely, a reversible reduction wave at −0.80 V was observed (vs $Ag/AgNO_3$ electrode).

For reference compound **L-1**, two reversible reduction waves at −0.45 and −0.64 V were observed (vs $Ag/AgNO_3$ electrode). No oxidation waves were observed within the potential range used in the electrochemical measurement. These results indicate that the PBI moiety in **B-1** is more likely an electron acceptor, rather than an electron donor. Moreover, the PBI moiety is more easily reduced than the 2,6-diiodoBodipy unit. Therefore, in a later discussion on the intramolecular electron transfer, the PBI moiety was considered as an electron acceptor and the diiodoBodipy moiety was treated as an electron donor.[32]

The redox potentials of **B-1** were compared with those of the components of the dyad, i.e. **L-3** and **L-1** (Figure 5). **L-3** and **B-1** show similar oxidation potentials. This result indicates that oxidation of the diiodoBodipy part was not affected by linking to the PBI moiety. For the reduction, however, the reduction wave of **B-1** is cathodically shifted in comparison to that of **L-3**. This result is reasonable, since the PBI moiety is reduced in a less negative range and, with the formation of the PBI anion, it is more difficult to inject the third electron into this dyad: i.e., into the diiodoBodipy moiety. The reduction waves of **B-1** were compared with those of **L-1**. The two compounds show identical reduction potentials (Table 2).

Table 2. Electrochemical Redox Potentials of the Compounds[a]

compound	oxidation (V)	reduction (V)
5	+1.43	−0.42, −0.62, −1.09
6	+1.43	−0.38, −0.60, −1.08
L-3	+1.52	−0.80
L-1	*b*	−0.45, −0.64
B-1	+1.57	−0.40, −0.61, −0.85
L-2	*b*	−0.45, −0.64
B-2	+1.57	−0.36, −0.60, −0.84

[a]Cyclic voltammetry in Ar-saturated CH_2Cl_2 containing a 0.10 M Bu_4NPF_6 supporting electrolyte. The counter electrode is Pt, and the working electrode is glassy carbon, with the $Ag/AgNO_3$ couple as the reference electrode. Conditions: *c* [Ag^+] = 0.1 M, 0.5 mM compounds in CH_2Cl_2, 25 °C. Ferrocene (Fc) was used as internal reference ($E_{1/2}$ = +0.64 V (Fc^+/Fc) vs standard hydrogen electrode. [b]Not observed.

The redox potentials of triad **B-2** were studied and were compared with those of the reference compounds **L-2** and **L-3** (Figure 6). Different from the case for **B-1**, the reduction waves of **B-2** are anodically shifted in comparison to that of **L-2**. A reversible oxidation wave at +1.57 V was recorded for **B-2**, which is assigned to the oxidation of the 2,6-diiodoBodipy. Three reversible reductive waves were observed at −0.36, −0.60 V and at −0.84 V, which are attributed to the 1,7-diphenylPBI moiety and the diiodoBodipy moiety, respectively. The redox potentials of the compounds are collected in Table 2. In comparison with **B-1** and **B-2**, similar redox potentials were observed for the uniodinated dyad **5** and triad **6** (Figure S47, Supporting Information).

It was reported that the triplet state of PBI derivatives can be produced by charge recombination.[63] Similar results were also observed with the Bodipy-C_{60} dyad and Si-phthalocyanine complex.[64] Therefore, the PET of the dyad and triad was studied. Electrochemical data were combined with the spectroscopic data to study the Gibbs free energy changes (ΔG°_{CS}) of the photoinduced electron transfer and the energy level of the charge transfer state (CTS) of **B-1** and **B-2**.

The free energy changes of the intramolecular electron transfer process can be calculated with the Weller equation (eqs 2 and

$$\Delta G^\circ_{CS} = e[E_{OX} - E_{RED}] - E_{00} + \Delta G_S \quad (2)$$

$$\Delta G_S = -\frac{e^2}{4\pi\varepsilon_S\varepsilon_0 R_{CC}} - \frac{e^2}{8\pi\varepsilon_0}\left(\frac{1}{R_D} + \frac{1}{R_A}\right)\left(\frac{1}{\varepsilon_{REF}} - \frac{1}{\varepsilon_S}\right) \quad (3)$$

3),[64a] where ΔG_S is the static Coulombic energy, which is described by eq 3, e = electronic charge, E_{OX} = half-wave potential for one-electron oxidation of the electron-donor unit, E_{RED} = half-wave potential for one-electron reduction of the electron-acceptor uni, E_{00} = energy level approximated with the fluorescence emission (for the singlet excited state), ε_S = static dielectric constant of the solvent, R_{CC} = center-to-center separation distance between the electron donor (diiodoBodipy) and electron acceptor (PBI), determined by DFT optimization of the geometry, R_{CC}(**B-1**) = 10.76 Å, R_{CC}(**B-2**) = 11.54 Å, R_D is the radius of the electron donor, R_A is the radius of the electron acceptor, ε_{REF} is the static dielectric constant of the solvent used for the electrochemical studies, and ε_0 is the permittivity of free space. The solvents used in the calculation of free energy of the electron transfer are toluene (ε_S = 2.38), CH_2Cl_2 (ε_S = 8.93), and acetonitrile (ε_S = 37.5).

Energies of the charge-separated states (E_{CS}) and charge recombination energy states (ΔG_{CR}) can be calculated with eqs 4 and 5. The data are collected in Table 3.

$$E_{CS} = e[E_{OX} - E_{RED}] + \Delta G_S \quad (4)$$

$$\Delta G_{CR} = -(\Delta G_{CS} + E_{00}) \quad (5)$$

The free energy changes of the intramolecular electron transfer and the charge recombination are compiled in Table 3. In principle, electron transfer is thermodynamically allowed, even in nonpolar solvents such as toluene. This prediction was confirmed by the quenching of the fluorescence of energy

DOI: 10.1021/jo502899p
J. Org. Chem. 2015, 80, 3036−3049

Table 3. Driving Forces of Charge Recombination (ΔG_{CR}) and Charge Separation (ΔG_{CS}) for the Dyad B-1, Triad B-2, and the Reference Compounds L-1, L-2, and L-3 in Toluene, Dichloromethane, and Acetonitrile

	$\Delta G_{CS}{}^{a}$ (eV)	$\Delta G_{CR}{}^{a}$ (eV)	$\Delta G_{CS}{}^{b}$ (eV)	$\Delta G_{CR}{}^{b}$ (eV)	$\Delta G_{CS}{}^{c}$ (eV)	$\Delta G_{CR}{}^{c}$ (eV)
B-1	−0.09[d]	−2.15	−0.42[d]	−1.82	−0.51[d]	−1.73
	0.00[e]		−0.33[e]		−0.42[e]	
B-2	−0.09[d]	−2.15	−0.45[d]	−1.79	−0.54[d]	−1.70
	+0.04[e]		−0.36[e]		−0.45[e]	
5	−0.37[d]	−2.03	−0.7[d]	−1.70	−0.79[d]	−1.61
	−0.12[e]		−0.45[e]		−0.54[e]	
6	−0.37[d]	−2.03	−0.73[d]	−1.67	−0.82[d]	−1.58
	−0.12[e]		−0.48[e]		−0.57[e]	

[a]In toluene. [b]In CH_2Cl_2. [c]In acetonitrile. [d]Via ^{1}BDP*. [e]Via ^{1}PBI*.

acceptors in dyad **B-1** and triad **B-2**, even in a nonpolar solvent such as toluene (Figure 3). The energy level of the CTS is close to or lower than the singlet state of ^{1}[PBI]*; thus, the quenching of the PBI emissions in **B-1** and **B-2** is rationalized.[32] The photophysics of the dyad (**B-1**) and the triad (**B-2**) can be fully rationalized with the electrochemical data. Similarly, PET is thermodynamically allowed for the uniodinated dyad **5** and triad **6** (Table 3).

2.4. Nanosecond Transient Absorption Spectroscopy: Triplet Excited States of Dyad B-1 and Triad B-2. In order to investigate the triplet excited state of the dyad (**B-1**) and the triad (**B-2**), the nanosecond transient absorption spectroscopy of the compounds was studied (Figure 7).

Upon 532 nm pulsed laser photoexcitation, a bleaching band at 533 nm was observed for **B-1**. This band overlaps with the transient absorption band in the range 400−650 nm. This excited state absorption (ESA) profile is a ypical $T_1 \rightarrow T_n$ absorption of the PBI triplet excited state.[53,65,66] The transient absorption spectra of **B-1** are devoid of any significant absorption bands at 700 nm; thus, the transient species detected are not due to the PBI radical anions.[62] The iodoBodipy part gives a drastically different transient absorption profile (Figure 7): for example, the bleaching band and the transient absorption band wavelength.[51,67]

The decay trace at 470 nm gives a triplet excited state lifetime of 150 μs (Figure 7b). This lifetime is much longer than that observed with PBI-containing Pt(II) complexes (0.246 μs)[68] or with a different complex (0.37 μs).[69] With the PBI-containing Ir(III) complex, for which the T_1 state is an intraligand triplet state (not the conventional MLCT state), we observed a triplet state lifetime of 22.3 μs.[66] The production of the PBI triplet state in these complexes is based on the heavy-atom effect of the transition-metal atoms. Interestingly, we observed a lifetime of the PBI triplet state up to 105.9 μs with the PBI-C_{60} dyad.[65] Therefore, we propose that the inherent triplet state lifetime of an organic chromophore, which is devoid of ISC, such as PBI, can be probed by a triplet energy transfer approach (or sensitizing method), as for **B-1**.[38] The heavy-atom effect will produce the triplet excited state of an organic chromophore, but the lifetime is highly likely to be reduced due to the enhanced ISC process.

Similar results were observed for **B-2** (Figure 7c,d), for which the T_1 state is localized on the PBI moiety, and the triplet state lifetime was determined as 148 μs. The bleaching band of **B-1** at 533 nm is more significant in comparison with that of **B-2**. This is due to the larger molecular absorption coefficient of **L-1** in comparison to that of **L-2**.

The nanosecond transient absorption spectra of **L-3** (2,6-diiodoBodipy) was also studied (Figure 7e), for which the transient bleaching and absorption motif is substantially different from those of **B-1** and **B-2**. For example, the intensity ratio of the bleaching band to the transient absorption bands is much larger than that observed with **B-1** and **B-2**.[51] These results give unambiguous support for the assignment of the T_1 state in **B-1** and **B-2** as the PBI-localized triplet excited state, not the Bodipy moiety localized triplet state.

Since we have shown that the triplet formation by the reference compound **L-1** is negligible (no nanosecond transient signal was detected for **L-1**, **L-2**, and the uniodinated analogue compounds **5** and **6**)[62] and that the T_1 state of the Bodipy moiety

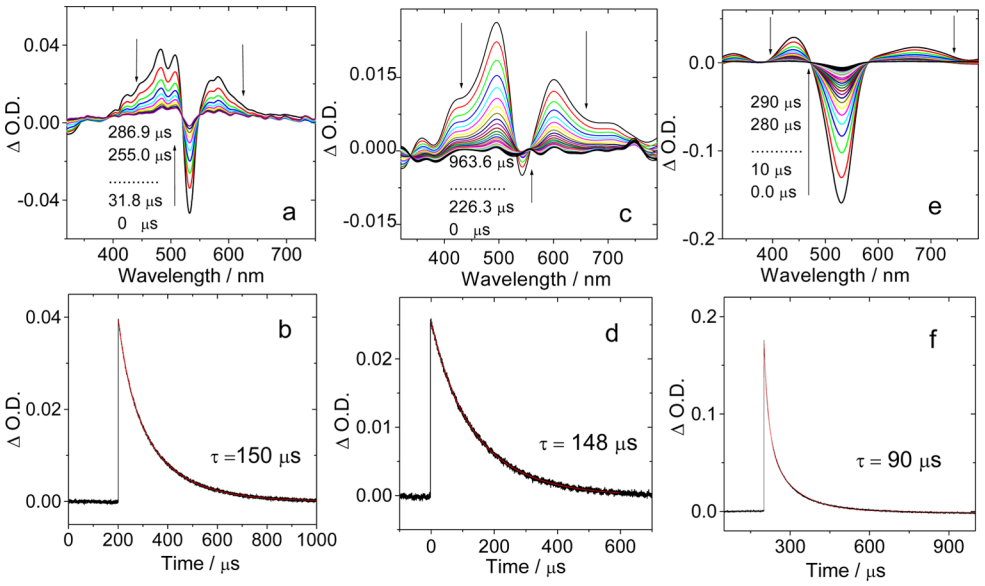

Figure 7. Nanosecond transient absorption of **B-1**, **B-2**, and **L-3**: (a) transient absorption spectra of **B-1**; (b) decay trace of **B-1** at 470 nm; (c) transient absorption difference spectra of **B-2**; (d) decay trace of **B-2** at 470 nm; (e) transient absorption difference spectra of **L-3**; (f) decay trace of **L-3** at 520 nm. Conditions: λ_{ex} 532 nm (nanosecond pulsed laser), $c = 1.0 \times 10^{-5}$ M in deaerated toluene, 20 °C.

DOI: 10.1021/jo502899p
J. Org. Chem. 2015, 80, 3036−3049

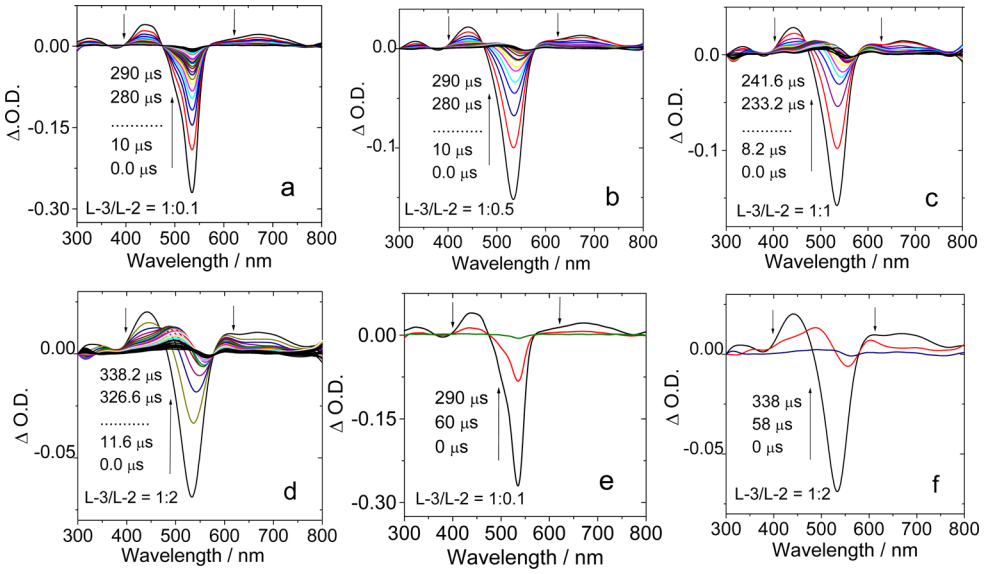

Figure 8. Intermolecular triplet energy transfer: nanosecond transient absorption spectra of a mixture of **L-2** and **L-3**, with **L-3** as the triplet energy donor and **L-2** as the triplet energy acceptor. The concentration of **L-3** is fixed at 1.0×10^{-5} M, and the concentration of **L-2** was increased to (a) 1.0×10^{-6} M, (b) 5.0×10^{-6} M, (c) 1.0×10^{-5} M, and (d) 2.0×10^{-5} M. (e) and (f) Selected transient absorption spectra at a few specific delay times, to show the faster TTET with greater **L-2**/**L-3** molar ratio. Conditions: excitation with a pulsed nanosecond laser at 532 nm, in deaerated toluene at 20 °C.

is 1.70 eV,[54] whereas the T_1 state of PBI is 1.2 eV,[53] as a result, Bodipy is the triplet energy donor and PBI is the triplet energy acceptor; thus, the production of a triplet state by **B-1** is most probably via intramolecular triplet state energy transfer (TTET) from iodo-Bodipy to the PBI unit. Since the intramolecular triplet energy transfer rate constant can be up to 10^9 s^{-1},[40,41] we postulate that these rate constants are applicable for **B-1** and **B-2**, in which the triplet energy donor (iodoBodipy) and the triplet energy acceptor (PBI) are in close vicinity, which is beneficial for the TTET (usually via the Dexter mechanism, i.e. electron exchange); thus, no slow development of the PBI transient feature can be detected with our nanosecond transient absorption spectrometer (the time resolution is 10 ns, which is unable to detect photophysical processes with rate constants larger than 10^8 s^{-1}).

It should be noted that intramolecular electron transfer was demonstrated by a steady-state fluorescence study, as well as electrochemical data. However, the triplet production by **B-1** and **B-2** was not affected significantly, concerning the aspects of both the triplet state lifetime of PBI and the triplet state yield (approximated by the singlet oxygen quantum yields; Table 1). Electrochemical data show that the CTS has an energy level of 1.82 eV (in CH_2Cl_2), which is well above the triplet state energy level of PBI (1.2 eV); thus, the triplet state of PBI is not perturbed by any electron transfer process.[71] Similar results were obtained with the solvents toluene and acetonitrile (Table 3).

Previously it was reported that the triplet state of PBI derivatives can be produced by charge recombination (CR).[63] Similar formation of the triplet state of C_{60} was observed with Bodipy-C_{60} dyad and Si-phthalocyanine complex.[64] However, for **B-1** and **B-2**, the triplet excited states of the PBI moiety were not populated via the CR process. Note that the electrochemical characterization (Table 3) and fluorescence spectra (Figures S44 and S45, Supporting Information) indicated PET for compounds **5** and **6**. However, no significant production of triplet excited states was observed for the uniodinated dyad **5** and the triad **6**.

2.5. Intermolecular Triplet Energy Transfer. Long-range energy transfer is important in many aspects; thus, we studied the *intermolecular* triplet state energy transfer between the 2,6-diiodoBodipy unit and the triplet acceptor PBI unit. The intermolecular triplet energy transfer was monitored by following the evolution of the transient of **L-3** upon increasing the concentration of **L-2** in the **L-2**/**L-3** mixture (Figure 8).[72] When the concentration of **L-2** was increased, the transient signal of **L-3** at 532 nm diminished more quickly, and the featured transient absorption spectrum of the PBI triplet state developed (Figure 8). For example, the bleaching band shifted from 530 to 556 nm with an increase in the concentration of **L-2** (Figure 8b–d). Concomitantly, the transient absorption band at 430 nm for diiodo-Bodipy disappeared and a new ESA band at 490 nm developed (Figure 8b–d), which is characteristic for the transient absorption of the triplet state of PBI. Changes were observed in the range 600–800 nm.

On the basis of these observations, we propose that intermolecular triplet–triplet energy transfer (TTET) occurred for the **L-2**/**L-3** mixture, with **L-3** as the triplet state energy donor and **L-2** as the triplet energy acceptor. No triplet state equilibrium was established due to the significant triplet state energy gap of iodoBodipy and the PBI moiety (ΔE = 0.5 eV). Similar intermolecular TTET was observed for a mixture of **L-3** and **L-1** with transient absorption spectra (Figure S48, Supporting Information). These results support the ultrafast intramolecular TTET in **B-1** and **B-2**.

In order to study the kinetics of the transient absorption evolvement for a mixture of **L-2** and **L-3**, i.e. the TTET process, the transient absorption (the ΔOD) at 500 nm was monitored (Figure 9).[72] **L-3** gives the ground-state bleaching at 500 nm; for **L-2**, however, ESA absorption was observed. Therefore, the most significant information will be attained by monitoring the decay trace at 500 nm, that is, the instant production of the triplet state of **L-3** and thereafter the formation of the triplet state of **L-2**. Therefore, in order to study the intermolecular triplet energy transfer between **L-3** and **L-2**, the decay trace of the mixture at 500 nm was monitored. The information revealed by the evolution of the transient at 500 nm includes the kinetic information on the decay of the triplet state of **L-3** (triplet energy

DOI: 10.1021/jo502899p
J. Org. Chem. 2015, 80, 3036–3049

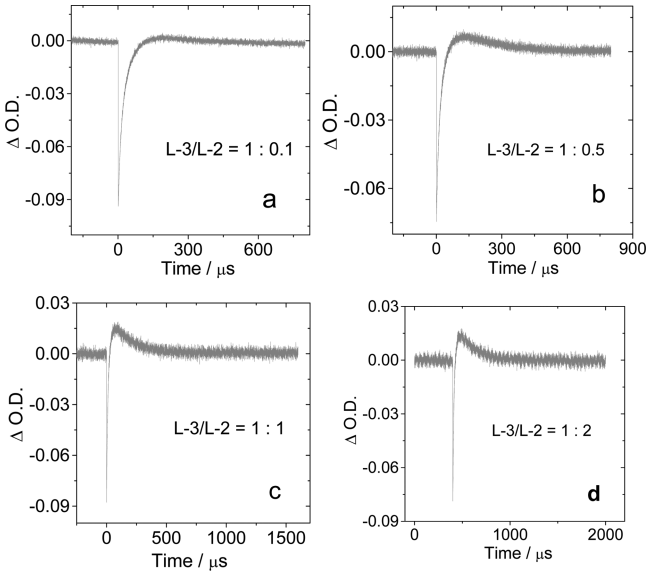

Figure 9. Comparison of decay curves at 500 nm for a mixture of **L-2** and **L-3** with different **L-3**/**L-2** molar ratios. The concentration of **L-3** was fixed at 1.0×10^{-5} M, and the concentration of **L-2** is (a) 1.0×10^{-6} M, (b) 5.0×10^{-6} M, (c) 1.0×10^{-5} M, and (d) 2.0×10^{-5} M. Conditions: in deaerated toluene at 20 °C.

donor) and finally the decay of the triplet excited state of **L-2** (the triplet energy acceptor). More importantly, the intermolecular TTET will be revealed by the ΔOD trace at 500 nm, i.e. the appearance of the positive ΔOD values. Therefore, the decay trace at 500 nm will reveal at least three photophysical processes.

At low **L-2** concentration, the decay of the transient of the **L-2**/**L-3** mixture is identical with that of the **L-3** alone (Figure 9a). Under this circumstance the intermolecular energy transfer is negligible (Figure 8b). Upon an increase in the concentration of **L-2**, following the normal recovery of the bleaching, the OD increased positively in the range 360−550 nm, indicating the significant production of the triplet state of PBI. Note that the triplet state of PBI shows a positive transient absorption at 500 nm.[65,66] Then the third phase of the trace at 500 nm indicated the decay of the triplet state of PBI. This three-phase feature of the decay trace at 500 nm becomes more distinct with an increas in the concentration of **L-2**: i.e., with more significant intermolecular TTET (Figure 9c,d).

The traces of the transient at 490 nm for **L-3** and the mixture of **L-3**/**L-2** (1/2 molar ratio) were compared (Figure 10). For **L-3**, a decay trace with a long lifetime of 90.5 μs was observed. In the

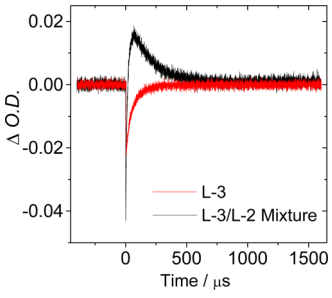

Figure 10. Comparison of the decay trace of **L-3** and the mixture of **L-3** and **L-2** at 490 nm upon nanosecond pulsed laser excitation. Conditions: c[**L-3**] = 1.0×10^{-5} M and c[**L-2**] = 2.0×10^{-5} M in deaerated toluene, at 20 °C.

presence of **L-2**, however, it is clear that the lifetime of the triplet state of iodoBodipy is much shorter, and significant production of the triplet state of PBI was observed, indicated by the production of a positive transient absorption at 490 nm. The latter decay trace at 490 nm is due to the decay of the T_1 state of **L-2**. Thus, these results indicated that the T_1 state of **L-2** was produced by the intermolecular TTET.[72]

2.6. Femtosecond Transient Absorption Spectroscopy. Ultrafast pump-probe experiments were performed for both **B-1** and **B-2** at 530 nm pump. It is expected that ultrafast spectroscopy studies will give evidence of singlet state intramolecular resonance energy transfer (RET) and formation of the triplet state of diiodo-BODIPY (via ISC) and PBI moieties in **B-1** and **B-2** (Figure 11).[64a,38] Although there are minor differences, compounds **B-1** and **B-2** both exhibit similar characteristics in their pump-probe data.

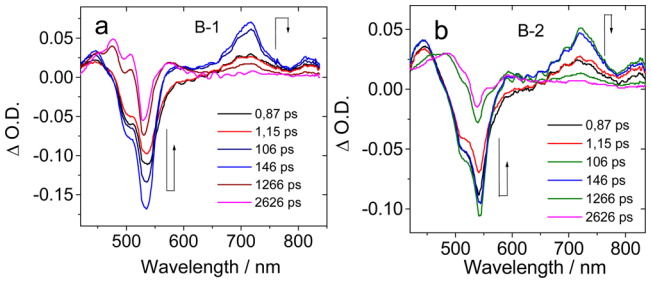

Figure 11. Ultrafast transient absorption spectra of (a) **B-1** and (b) **B-2**. Conditions: c = 1.0×10^{-5} M in toluene, excited with 530 nm femtosecond pulsed laser, 20 °C.

The iodo-BODIPY and the PBI moieties were both excited with a pump beam instantaneously due to overlapping of absorption bands, indicated by the bleaching bands in the range 450−650 nm (centered at 530 nm, Figure 11). This bleaching signal represents depletion of singlet states of both the diiodo-BODIPY and the PBI moieties. The 530 nm bleaching signal decreases until about 2 ps and increases from 2 to 250 ps, as presented in Figure 11. This behavior could be due to competition between FRET from iodo-BODIPY to PBI and ISC of iodo-BODIPY mechanisms.

There are several positive signals (ESA) in the ultrafast pump probe spectra representing transient absorptions in the investigated samples (Figure 11). The absorption around the 420 nm region occurring simultaneously with the pump pulse is attributed to the $S_1 \rightarrow S_n$ transition of the diiodo-BODIPY moiety. Another simultaneous transient absorption signal with the pump pulse is observed around the 720 nm region. The transient absorption band centered at 710 nm (**B-1**) or 725 nm (**B-2**) is due to the $S_1 \rightarrow S_n$ absorption of the PBI moieties in **B-1** and **B-2**.[73−75] It should be noted that the radical anion of PBI also shows transient absorption in the same region.[62] However, the position of the transient absorption bands at 710/725 nm did not change during 0−2626 ps after excitation; thus, it is unlikely that other species, such as the radical anion $PBI^{\bullet-}$, were produced via the singlet excited state of PBI.[75] Moreover, an intermolecular interaction, such as the $\pi-\pi$ stacking, can be excluded since the transient absorption band at 710 nm is not broad.[75] The fact that this signal increases after 2 ps until about 250 ps indicates that there is FRET from iodo-BODIPY to the PBI moiety (Figure 11).

In order to reveal the kinetics of the photophysical processes in detail, the decay traces at a few critical wavelengths were

DOI: 10.1021/jo502899p
J. Org. Chem. 2015, 80, 3036−3049

monitored (Figure 12). For both **B-1** and **B-2**, the decay trace at 715 and 725 nm had a triple-phase feature (Figure 12b). The

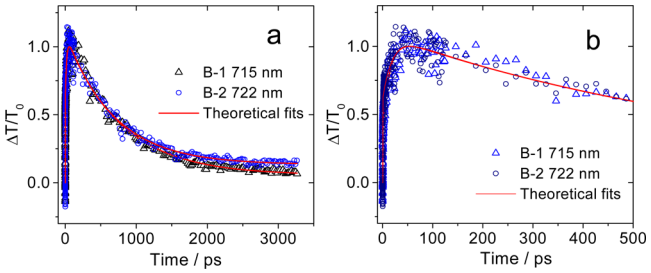

Figure 12. (a) Decay curves of **B-1** and **B-2** at 715 and 722 nm probe wavelength, respectively. (b) Magnified early stage of the decay curves to show the triple-phase feature. The data are derived from parts a and b of Figure 11, respectively.

quickly increasing phase of the curves is due to the instant excitation of the PBI moiety in **B-1** and **B-2** upon femtosecond pulsed laser excitation. Then a relatively slow increasing phase was observed, which is complete within ca. 50 ps. This process is due to the production of a PBI singlet excited state via FRET, with the diiodoBodipy unit as the singlet energy donor. The rate constant for this process is ca. $k_{RET} = 5 \times 10^{10}$ s^{-1} for **B-1**. Previously, a larger value was reported for the Bodipy-azaBodipy triad (ca. 1.0×10^{11} s^{-1}).[32] For Bodipy-styrylBodipy triads, the calculated k_{RET} value is up to 2.3×10^{11} s^{-1}.[60] In a bichromic Bodipy-Pt(porphyrin) complex, the singlet energy transfer rate constant is up to 7.8×10^{11} s^{-1}.[40] The relatively slow FRET may be attributed to the poor spectral overlap between the emission of the diiodoBodipy part and the absorption of the PBI moiety.[3,30,76−78]

The third phase of the decay curve, i.e. the decay of the transient absorption at 710/725 nm, is slow (Figure 12b). The rate constant for this decay process was approximated as $k = 1 \times 10^9$ s^{-1}. The lifetime of this transient is ca. 1 ns, which is very close to the fluorescence lifetimes of **B-1** and **B-2** determined in separate experiments (i.e., the lifetime of the emissive singlet excited state, 0.96 or 0.84 ns, Table 1). These results, and the electrochemical characterization data, all support that the transient absorption at 710/725 nm is due to the singlet excited state of PBI,[73] for which three phases were observed: i.e., the instant production of the PBI singlet excited state by excitation and then by FRET and finally the decay of the S_1 state to the ground state (S_0 state).

The decay traces of the transient in the characteristic region (450−650 nm) of the triplet excited state of PBI were also monitored (Figure 13).[53,65,66,70] For **B-1**, the fast development of the bleaching at 507 nm is due to the prompt excitation of the diiodoBodipy unit upon femtosecond laser excitation. Thereafter a slow increasing of the bleaching was observed; the process was finished in ca. 100 ps. A few photophysical manifolds may be involved in this slow process, such as the FRET, intersystem crossing of diiodoBodipy and the following TTET from diiodoBodipy to the PBI moiety. The rationalization for this postulation is given in the following section. First, the steady-state absorption wavelengths of PBI and the diiodoBodipy moiety are similar to each other (Figure 11); thus, no clear trend for the change of the transient absorption at 507 nm can be observed with the FRET process. Second, the intersystem crossing of diiodoBodipy ($k_{ISC} = 7.7 \times 10^9$ s^{-1}, 130 ps)[61] will not significantly alter the bleaching band of diiodoBodipy at 507 nm:

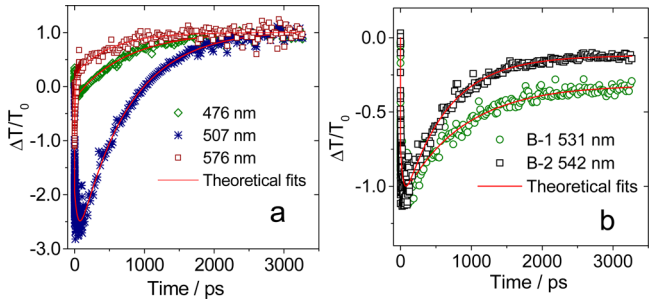

Figure 13. (a) Comparison of decay curves of **B-1** at 476, 507, and 576 nm, respectively. (b) Comparison of decay curves of **B-1** and **B-2** at 531 and 542 nm, respectively. The data are extracted from Figure 11.

i.e., the ΔOD value will not change with time. Third, after the ISC of diiodoBodipy, intermolecular TTET to PBI may occur; thus, the bleaching band intensity will decrease because the steady-state absorption of PBI in the region 475−600 nm is much weaker than that of the diiodoBodipy part. All of these processes may result in a complicated kinetics in the time range 1−100 ps (Figure 13a).

On the basis of the above analysis, the FRET process takes about 50 ps to finish, which is in agreement with the result derived from the transient absorption at 710 nm. Thus, the rate constant of the FRET process can be determined as $k_{RET} = 5 \times 10^{10}$ s^{-1}.[62] After 100 ps, the bleaching band at 507 nm decreased and recovered toward the baseline. We noted that the singlet state of the PBI moiety does not absorb at this wavelength,[62,73−75] Instead, the triplet state of PBI absorbs at this wavelength.[53,65,70] On the other hand, the triplet state of diiodoBodipy does not absorb at 507 nm (Figures 7 and 8).[61] Therefore, we conclude that the recover of the bleaching at 507 nm is due to the consumption of the triplet state of diiodoBodipy and the production of the triplet state of PBI: i.e. the intramolecular triplet state energy transfer. This downhill TTET was supported by the *intermolecular* TTET studied with nanosecond transient absorption spectroscopy (vide supra). Interestingly, this is a slow process which takes ca. 1 ns; thus, the rate constant of the intramolecular TTET was estimated as $k_{TT} = 1 \times 10^9$ s^{-1}. Previously for a bichromic Bodipy-Pt(porphyrin) hybrid, the intramolecular TTET process was reported with a rate constant of $k_{TT} = 1.0 \times 10^{10}$ s^{-1}.[40] For a Bodipy-*N*^*N* Pt(II) complex, the k_{TT} value is up to 6.0×10^{10} s^{-1}.[41] A much slower TTET was found for a hydrogen-bonding C_{60}-ferrocene assembly ($k_{TT} = 9.2 \times 10^5$ s^{-1}).[56]

On the other hand, there are transient absorption signals appearing after 100 ps. A similar observation is also valid for a transient absorption around 830 nm. Therefore, this signal could be related to the $S_1 \rightarrow S_n$ transition of PBI moieties as well. The transient absorption spectrum of **B-1** has three positive signals at 480, 505, and 575 nm appearing at delay times of 250, 1000, and 100 ps, respectively (Figure 13). The lifetimes of these signals are on the order of microseconds (Figure 13), and therefore these signals can be attributed to $T_1 \rightarrow T_n$ transitions.[53,65,70] A transient absorption signal appearing at the earliest time at 575 nm can be attributed to the $T_1 \rightarrow T_n$ transition of iodo-BODIPY. We expect the $T_1 \rightarrow T_n$ transition related with this state to be delayed in comparison to the $T_1 \rightarrow T_n$ transition of iodo-BODIPY. This is why the transient absorption signal appearing at a later time at 505 nm is attributed to the $T_1 \rightarrow T_n$ transition of PBI. Note that the amplitude of the $T_1 \rightarrow T_n$ transition of iodo-BODIPY is smaller than that of other transient absorption signals

DOI: 10.1021/jo502899p
J. Org. Chem. 2015, 80, 3036−3049

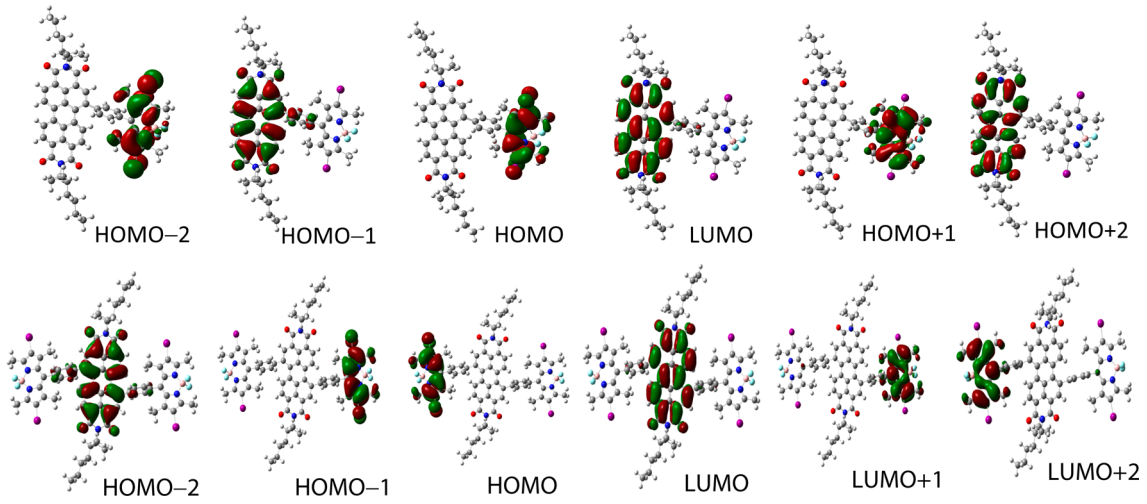

Figure 14. Selected frontier molecular orbitals of compounds **B-1** (upper row) and **B-2** (lower row). The calculations are based on the optimized ground state geometry (S_0 state) at the B3LYP/6-31G(d)/level using Gaussian 09W.

after 100 ps; this may be more proof that ISC of the iodo-BODIPY is quenched to some extent by FRET.

These transient absorption signals of **B-2** are slightly different from those of **B-1.** The two bands around 480 and 505 nm become a single absorption band for the **B-2** sample due to the presence of two iodo-BODIPY groups. The other differences between **B-1** and **B-2** are the lifetimes of the bleaching signals around 530 nm. The **B-2** sample exhibits a faster and therefore more efficient energy transition due to the two donor iodo-BODIPY moieties (Figure 13b). This result may be the reason **B-2** shows more efficient fluorescence quenching than **B-1**, as seen from fluorescence measurements (Figure 2).

In summary, the rate constant of the FRET and the ISC of **B-1** indicated that 87% of the singlet excited state of diiodoBodipy in **B-1** will decay via FRET, whereas 13% of the singlet excited state of diiodoBodipy will decay via ISC, as estimated by the respective rate constants of the two processes. However, the decay curves at 710 nm and the singlet oxygen sensitizing experiments (Φ_Δ = 80%, Table 1) all show that a much smaller ratio of FRET/ISC is occurring for **B-1**. We confirmed that the triplet yield via CR is negligible with the uniodinated reference compounds **5** and **6**. Thus, we postulate that the singlet excited state of diiodoBodipy may be trapped by some unknown mechanisms, such as a vibrational barrier (or small Franck−Condon factor), to prevent a complete FRET from occurring.[79] A detailed investigation of this issue requires extensive theoretical calculations which are beyond the scope of this paper.

2.7. DFT Calculations. The ground state geometries of **B-1** and **B-2** were optimized with the DFT method (Figure 14). The phenyl ring, as a linker between the PBI and the BODIPY moieties, takes a perpendicular geometry toward the two moieties. Thus, the Bodipy moiety and the PBI moiety in the dyad and triad are almost coplanar. However, the frontier molecular orbitals of **B-1** and **B-2** show that there is no π conjugation between the Bodipy and PBI moieties. Moreover, for dyad **B-1**, HOMO is localized on the Bodipy moiety, whereas the LUMO is confined on the PBI moiety. Thus, photoinduced electron transfer is the feature of the electronic transition upon photoexcitation. This conclusion is in full agreement with the weak fluorescence of **B-1** (quenching of the PBI moiety emission in **B-1**), as compared with that of compound **5** (Figure 3a). Similar DFT calculation results were observed for **B-2** (Figure 14).

The spin density surfaces of the dyad **B-1** and triad **B-2** were calculated with DFT methods (Figure 15). The spin density surface of the dyad/triad will indicate the localization of triplet excited states. The DFT calculation results show that the triplet excited states of **B-1** and **B-2** are exclusively confined on the PBI moiety, not the Bodipy moiety. These theoretical results are in full agreement with what we observed with nanosecond transient absorption spectroscopy, which indicated that the triplet excited states of **B-1** and **B-2** are exclusively localized on the PBI moiety and the Bodipy moiety does not contribute to the triplet excited states of **B-1** and **B-2** (Figure 7).

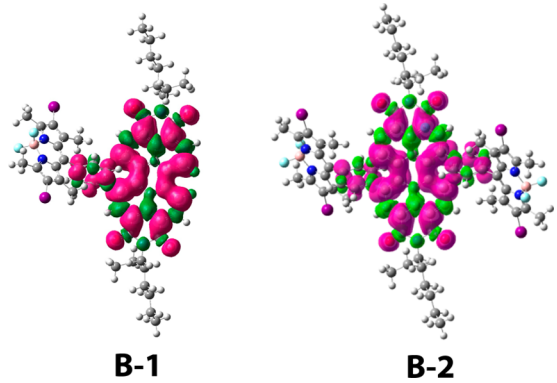

Figure 15. Isosurfaces of spin density of PBI-BODIPY sensitizers **B-1** and **B-2**. Calculations were performed at the B3LYP/6-31G(d) level with Gaussian 09W.

2.8. Energy Level Diagram and the Photophysical Processes. On the basis of the spectral and electrochemical data, the energy levels of the excited states, as well as the photophysical processes, are summarized in Scheme 2 (exemplified with **B-1**). Upon excitation into the diiodoBodipy unit, ultrafast FRET competes with the ISC of the diiodoBodipy moiety. In CH_2Cl_2, the CTS lies below the S_1 state of the PBI moiety; as a result, the fluorescence of the PBI unit should be significantly quenched. This postulation is in agreement with the fluorescence of **B-1** (Figure 3). Note that the PBI moiety shows very weak ISC, supported by the high fluorescence of the reference compound

DOI: 10.1021/jo502899p
J. Org. Chem. 2015, 80, 3036−3049

Scheme 2. Simplified Jablonski Diagram Illustrating the Photophysical Processes Involved in B-1 (in CH_2Cl_2)[a]

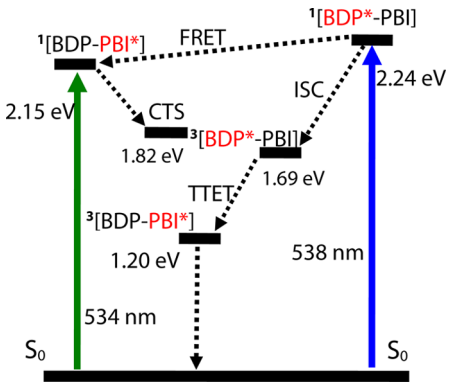

[a]The energy levels of the excited state are derived from the spectroscopic data and the electrochemical data. [BDP-PBI] stands for the diiodoBodipy and PBI units in **B-1**. The component at the excited state is designated in red. The number of the superscript designates the spin multiplicity.

L-1 (42.4%, Table 1) and the low singlet oxygen quantum yields (Φ_Δ = 0.08). The charge recombination does not likely produce the PBI triplet state efficiently, indicated by the results of the references dyad **5** and triad **6** (iodo-free). Furthermore, the dyad **B-1** and triad **B-2** do not show any $^1O_2$ photosensitizing ability in dichloromethane and acetonitrile, indicating that the triplet excited state is not produced by the charge recombination (CR). Excitation into the PBI moiety will give a similar photophysical process, except for the lack of FRET. Since the CTS lies well above the T_1 state of the PBI unit, the production of the triplet state is not affected by CTS; for example, the lifetime of the triplet state **B-1** is very long and the triplet state yield is high (Φ_Δ = 0.80 for **B-1**, Table 1). Similar photophysical processes were proposed for **B-1** in toluene and acetonitrile (see the Supporting Information, Schemes S49 and S50); note that the fluorescence of the PBI moiety in **B-1** was quenched under these circumstances, but not the triplet state of the PBI moiety. Similar photophysical processes were proposed for **B-2** (see the Supporting Information, Figures S54 and S55). Thus, the photophysical properties of **B-1**, such as the quenching of the fluorescence of the PBI unit, the ultrafast FRET yet high triplet yield (approximated by the singlet oxygen yield of **B-1**), and the independence of the triplet state property of solvent polarity, are fully rationalized by the excited state and the CTS energy levels.

2.9. Conclusion. In summary, diiodoBodipy-perylenebisimide dyads/triads were prepared, in order to study the competing intersystem crossing (ISC) and resonance energy transfer (RET) processes. The diiodoBodipy part is the singlet energy donor and, at the same time, the spin converter to produce a triplet state upon photoexcitation. The PBI moiety is the singlet/triplet energy acceptor; as a result, the ISC of the diiodoBodipy moiety competes with RET. With steady state and femto/nanosecond transient absorption and steady state fluorescence spectroscopy, we demonstrated the singlet energy transfer and electron transfer for these iodinated dyad and the triad. ISC is not completely outcompeted by the intramolecular RET process. On the basis of electrochemical data, the charge transfer state (CTS) is identified residing between the S_1 state and the T_1 state of the PBI moiety; thus, the fluorescence of PBI in the dyad and triad is drastically quenched in comparison with the reference PBI compound, yet the triplet state of the PBI is not affected by the CTS. Since the PBI moiety has a T_1 state energy level (1.2 eV) much lower than that of Bodipy moiety (1.7 eV), the triplet−triplet energy transfer (TTET) process produces the PBI triplet state, and an exceptionally long-lived triplet state lifetime was observed (150 μs). Previously the triplet state lifetime of PBI observed with a Pt(II) coordination approach was much shorter (<1 μs). Thus, we propose to use the TTET approach, instead of the conventional heavy-atom effect, to study the inherent triplet state properties of organic chromophores which are devoid of ISC capability. The intermolecular triplet state energy transfer was studied with nanosecond transient absorption spectroscopy. The intramolecular triplet energy transfer is ultrafast ($k_{TT} > 10^8$ s^{-1}), whereas the intermolecular TTET is relatively slow. The FRET effect of the dyad and the triad was studied with femtosecond pump-probe transient absorption spectroscopy, which indicates that the FRET has a rate constant of 5×10^{10} s^{-1}. Previously the ISC of the diiodoBodipy moiety was determined with much slower kinetics ($k_{ISC} = 7.7 \times 10^9$ s^{-1}). Thus, we propose the singlet excited state of the energy donor of the RET is trapped somehow from undertaking the fast FRET process. Moreover, with uniodinated reference dyad and triad, we confirmed that the triplet excited state localized on the PBI moiety is not produced by charge recombination. This information will be useful for designing multichromophore organic triplet photosensitizers and inspiring in-depth insights into the fundamental photophysical processes of multichromophore molecular assemblies.

3. EXPERIMENTAL SECTION

3.1. Analytical Measurements. All of the chemicals used in synthesis are analytically pure and were used as received. Solvents were dried and distilled before use for synthesis. Luminescence quantum yields of the compounds were measured with **L-3** as the standard (Φ_F = 2.7% in CH_3CN).

3.2. Synthesis of Compound 1. The mixture of 3,4,9,10-pyrelenetetracarboxylic dianhydride (2.0 g, 5.1 mmol), imidazole (10.0 g, 146.9 mmol), and 2-ethylhexylamine (3.8 mL, 21.0 mmol) was stirred under an Ar atmosphere at 160 °C for 6 h. Then the mixture was cooled and chloroform was added. The organic layer was dried, and the solvent was evaporated under reduced pressure. The crude product was not further purified and was directly used in the next reaction. Mp: > 250 °C. ^{1}H NMR ($CDCl_3$, 500 MHz): δ 8.56 (d, 4H, J = 5.0 Hz), 8.44 (d, 4H, J = 5.0 Hz), 4.17−4.09 (m, 4H), 1.98−1.93 (m, 2H), 1.43−1.33 (m, 16H), 0.97 (t, 6H, J = 7.2 Hz), 0.91 (t, 6H, J = 7.09 Hz). TOF MALDI-HRMS: calcd ($[C_{40}H_{42}N_2O_4]^-$), m/z 614.3145; found, m/z 614.3186.

3.3. Synthesis of Compound 2. Under an Ar atmosphere, a mixture of *N*,*N*′-bis(2-ethylhexan-1-amine)perylene-3,4,9,10-tetracarboxylic dianhydride (2.0 g, 3.3 mmol), bromine (9.0 mL, 180.0 mmol), and chloroform (50 mL) was stirred at room temperature for 48 h. The mixture was washed with saturated $Na_2S_2O_3{\cdot}5H_2O$ aqueous solution. The organic layer was dried over anhydrous Na_2SO_4, and the solvent was removed under reduced pressure. The residue was purified with column chromatography (silica gel, CH_2Cl_2) to give a red solid (500 mg, yield 22%). Mp: > 250 °C. ^{1}H NMR ($CDCl_3$, 500 MHz): δ 9.73 (d, 1H, J = 5.0 Hz), 8.85 (s, 1H), 8.64 (d, 3H, J = 5.0 Hz), 8.52 (d, 2H, J = 8.2 Hz), 4.18−4.07 (m, 4H), 1.98−1.92 (m, 2H), 1.42−1.32 (m, 16H), 0.97−0.89 (m, 12H). TOF HRMS ESI: calcd ($[C_{40}H_{41}N_2O_4Br]^+$), m/z 692.2250; found, m/z 692.2245.

3.4. Synthesis of Compound 3. Under an Ar atmosphere, a mixture of *N*,*N*′-bis(2-ethylhexan-1-amine)perylene-3,4,9,10-tetracarboxylic dianhydride (2.0 g, 3.3 mmol), bromine (9.0 mL, 180.0 mmol), and chloroform (50 mL) was stirred at 60 °C for 48 h. The mixture was washed with saturated $Na_2S_2O_3{\cdot}5H_2O$ aqueous solution. The organic layer was dried over anhydrous Na_2SO_4, and then the solvent was evaporated under reduced pressure. The residue was purified with

DOI: 10.1021/jo502899p
J. Org. Chem. 2015, 80, 3036−3049

column chromatography (silica gel, CH_2Cl_2) to give a red solid (760 mg, yield 30%). Mp: > 250 °C. ^{1}H NMR ($CDCl_3$, 500 MHz): δ 9.46 (d, 2H, J = 8.0 Hz), 8.90 (s, 1H), 8.67 (d, 2H, J = 8.0 Hz), 4.19−4.09 (m, 4H), 1.97−1.92 (m, 2H), 1.42−1.32 (m, 16H), 0.97−0.89 (m, 12H). TOF MALDI-HRMS: calcd ($[C_{40}H_{40}N_2O_4Br_2]^-$), m/z 770.1355; found, m/z 770.1373.

3.5. Synthesis of Compound 4. Under an Ar atmosphere, 4-formylbenzeneboronic acid (1.50 g, 10.0 mmol) and pinacol (1.18 g, 10 mmol) were placed with toluene (150 mL) in a round-bottom flask. The mixture was refluxed for 12 h at 120 °C. Evaporation of the solvent under reduced pressure lead to formation of a white-yellow solid (2.3 g, yield 99%). This crude product was used for the next step of the synthesis without further purification.

Under an Ar atmosphere, the above crude product (2.0 g, 8.7 mmol) and 2,4-dimethylpyrrole (2 mL, 20 mmol) were dissolved in dry CH_2Cl_2 (150 mL). A few drops of trifluoroacetic acid were added to the solution, and the mixture was stirred overnight at room temperature. After completion of the reaction (monitored via TLC), a solution of DDQ (2.0 g, 8.7 mmol) in freshly distilled THF was added to the reaction mixture. The reaction mixture was stirred for 2 h. Absolute triethylamine (10 mL) was added to the reaction mixture. After this mixture was stirred for 15 min, $BF_3{\cdot}Et_2O$ (10 mL) was added dropwise under ice-cold conditions. After the reaction mixture was stirred for 2 h more, the mixture was washed with water several times and then extracted with DCM. The organic phase was dried over anhydrous Na_2SO_4, and then the solvent was evaporated under reduced pressure. The residue was purified with column chromatography (silica gel, CH_2Cl_2) to give a red solid (1.2 g, yield 31%). ^{1}H NMR ($CDCl_3$, 500 MHz): δ 7.91 (d, 2H, J = 5.0 Hz), 7.30 (d, 2H, J = 5.0 Hz), 5.97 (s, 2H), 2.55 (s, 6H), 1.39 (s, 12H), 1.37 (s, 6H). TOF MALDI-HRMS: calcd ($[C_{25}H_{30}N_2O_2B_2F_2]^+$), m/z 450.2461; found, m/z 450.2446.

3.6. Synthesis of Compound 5. Under an Ar atmosphere, compound **2** (110.0 mg, 0.15 mmol), compound **4** (70.0 mg, 0.15 mmol), K_2CO_3 (65.0 mg, 0.45 mmol), and EtOH/toluene/water (50 mL, 2/4/1, v/v) were mixed together. Then $Pd(PPh_3)_4$ (9.0 mg, 0.007 mmol, 5 mol %) was added. The reaction mixture was refluxed and stirred under Ar for 8 h. After completion of the reaction, the mixture was cooled to room temperature. The reaction mixture was extracted with CH_2Cl_2, washed with water (2 × 100 mL), and dried over Na_2SO_4. The solution was evaporated to dryness under reduced pressure to give a crude solid. The crude product was further purified with column chromatography (silica gel, CH_2Cl_2) to give an orange solid (80 mg, yield 57%). Mp: > 250 °C. ^{1}H NMR ($CDCl_3$, 400 MHz): δ 8.74−8.62 (m, 4H), 8.58 (s, 1H), 8.05 (dd, 2H, J_1= 8.0 Hz, J_2 = 24 Hz), 7.69 (d, 2H, J = 8.0 Hz), 7.52 (d, 2H, J = 8.0 Hz), 6.14 (s, 1H), 6.04 (s, 1H), 4.21−4.06 (m, 4H), 2.60 (d, 6H, J = 8.0 Hz), 1.99−1.93 (m, 2H), 1.45−1.30 (m, 16H), 1.25 (s, 6H), 0.98−0.88 (m, 12H). ^{13}C NMR (100 MHz, $CDCl_3$): δ 163.7, 163.5, 156.2, 143.9, 143.1, 140.6, 140.4, 136.1, 135.6, 134.9, 134.5, 134.3, 132.7, 131.3, 130.4, 130.2, 129.6, 129.0, 128.5, 128.0, 127.5, 123.8, 123.3, 123.1, 123.0, 122.7, 122.4, 121.6, 44.4, 38.1, 30.8, 29.7, 28.7, 24.1, 23.1, 14.7, 14.1, 10.7. TOF MALDI-HRMS: calcd ($[C_{59}H_{59}BN_4O_4F_2]^-$), m/z 936.4597; found, m/z 936.4595.

3.7. Synthesis of Compound 6. Under an Ar atmosphere, compound **3** (116.0 mg, 0.15 mmol), compound **4** (135.0 mg, 0.3 mmol), K_2CO_3 (125.0 mg, 0.9 mmol), and EtOH/toluene/water (50 mL, 2/4/1, v/v) were mixed together. Then $Pd(PPh_3)_4$ (9.0 mg, 0.007 mmol, 5 mol %) was added. The reaction mixture was refluxed and stirred under Ar for 8 h. After completion of the reaction, the mixture was cooled to room temperature. The reaction mixture was extracted with CH_2Cl_2, washed with water (2 × 100 mL), and dried over Na_2SO_4. The solution was evaporated to dryness under reduced pressure to give a crude solid. The crude product was further purified with column chromatography (silica gel, CH_2Cl_2) to give a solid (120 mg, yield 64%). Mp: >250 °C. ^{1}H NMR ($CDCl_3$, 500 MHz): δ 8.66 (s, 2H), 8.05 (dd, 4H, J_1 = 8.0 Hz, J_2 = 16 Hz), 7.76 (d, 4H, J = 8.0 Hz), 7.51 (d, 4H, J = 8.0 Hz), 6.09 (d, 4H, J = 40 Hz), 4.18−4.09 (m, 4H), 2.60 (s, 12H), 1.97−1.92 (m, 2H), 1.43−1.32 (m, 16H), 1.25 (s, 12H), 0.97−0.88 (m, 12H). ^{13}C NMR (100 MHz, $CDCl_3$): δ 163.8, 163.5, 156.2, 143.3, 140.3, 135.7, 135.6, 134.7, 133.9, 133.1, 132.6, 130.6, 130.3, 130.0, 129.8, 129.3, 127.9, 122.5, 122.4, 121.7, 44.5, 38.1, 31.9, 30.8, 29.7, 28.8, 24.1, 23.1, 14.7, 14.1, 10.7. TOF MALDI-HRMS: calcd ($[C_{78}H_{76}B_2N_6O_4F_4]^-$), m/z 1258.6050; found, m/z 1258.6025.

3.8. Synthesis of Compound L-1. Under an Ar atmosphere, compound **2** (110.0 mg, 0.15 mmol), phenylboronic acid (18.0 mg, 0.15 mmol), K_2CO_3 (65.0 mg, 0.45 mmol), and EtOH/toluene/water (50 mL, 2 4 1, v/v) were mixed together. Then $Pd(PPh_3)_4$ (9.0 mg, 0.007 mmol, 5 mol %) was added. The reaction mixture were refluxed and stirred under Ar for 8 h. After completion of the reaction, the mixture was cooled to room temperature. The reaction mixture was extracted with CH_2Cl_2, and the organic layer was washed with water (2 × 100 mL) and dried over Na_2SO_4. The solvent was evaporated to dryness under reduced pressure to give a crude solid. The crude product was further purified with column chromatography (silica gel, CH_2Cl_2) to give a red solid (58 mg, yield: 56%). Mp: >250 °C. ^{1}H NMR ($CDCl_3$, 400 MHz): δ 8.56−8.69 (m, 5H), 8.10 (d, 1H, J = 10.0 Hz), 7.83 (d, 1H, J = 10.0 Hz), 7.54−7.47 (m, 5H), 4.20−4.05 (m, 4H), 1.98−1.90 (m, 2H), 1.42−1.29 (m, 16H), 0.96−0.87 (m, 12H). ^{13}C NMR (100 MHz, $CDCl_3$) δ 163.9, 163.7, 142.5, 141.7, 136.1, 134.8, 134.7, 134.4, 132.5, 131.0, 130.9, 130.4, 130.1, 130.0, 128.9, 128.7, 128.4, 128.3, 128.0, 127.4, 123.5, 123.2, 123.1, 122.6, 122.2, 44.3, 38.0, 30.8, 28.7, 24.1, 23.1, 14.1, 10.6. TOF MALDI-HRMS: calcd ($[C_{46}H_{46}N_2O_4]^-$), m/z 690.3458; found, m/z 690.3463.

3.9. Synthesis of L-2. Under an Ar atmosphere, compound **3** (116.0 mg, 0.15 mmol), phenylboronic acid (36.0 mg, 0.3 mmol), K_2CO_3 (125.0 mg, 0.9 mmol), and EtOH/toluene/water (50 mL, 2/4/1, v/v) were mixed together. Then $Pd(PPh_3)_4$ (9.0 mg, 0.007 mmol, 5 mol %) was added. The reaction mixture was refluxed and stirred under Ar for 8 h. After completion of the reaction, the mixture was cooled to room temperature. The reaction mixture was extracted with CH_2Cl_2, the organic layer was washed with water (2 × 100 mL), and the organic layers were dried over Na_2SO_4. The solution was evaporated to dryness under reduced pressure to give a crude solid. The crude product was further purified with column chromatography (silica gel, CH_2Cl_2/petroleum ether 3/1, v/v) to give a solid (60 mg, yield 52%). Mp: >250 °C. ^{1}H NMR ($CDCl_3$, 500 MHz): δ 8.59 (s, 2H), 8.12 (d, 2H, J = 5.0 Hz), 7.77 (d, 2H, J = 10.0 Hz), 7.55−7.46 (m, 10H), 4.17−4.08 (m, 4H), 1.95−1.90 (m, 2H), 1.40−1.29 (m, 16H), 0.95−0.87 (m, 12H). ^{13}C NMR (100 MHz, $CDCl_3$): δ 163.8, 142.0, 141.1, 135.4, 134.8, 132.5, 130.3, 130.2, 129.4, 129.1, 129.0, 128.7, 127.6, 122.2, 121.8, 44.2, 37.9, 30.7, 28.7, 24.0, 23.1, 14.2, 10.6. TOF MALDI-HRMS: calcd ($[C_{52}H_{50}N_2O_4]^-$), m/z 766.3771; found, m/z 766.3750.

3.10. Synthesis of L-3. To a solution of Bodipy (200.0 mg, 0.62 mmol) in anhydrous CH_2Cl_2 (25 mL) was added excess *N*-iodosuccinimide (NIS. 558.0 mg, 2.48 mmol). The mixture was stirred at room temperature for about 30 min. After completion of the reaction, the mixture was washed with saturated $Na_2S_2O_3{\cdot}5H_2O$ aqueous solution and was extracted with DCM. The organic layer was dried over anhydrous Na_2SO_4, and then the solvent was evaporated under reduced pressure. The residue was purified with column chromatography (silica gel, CH_2Cl_2/petroleum ether, 2/1, v/v) to give a red solid (325 mg, yield 91%). Mp: 194.3−194.9 °C. ^{1}H NMR ($CDCl_3$, 500 MHz): δ 7.53−7.50 (m, 3H), 7.26−7.24 (m, 2H), 2.65 (s, 6H), 1.38 (s, 6H). ^{13}C NMR (100 MHz, $CDCl_3$) δ 156.8, 145.4, 141.4, 134.8, 131.3, 129.6, 129.5, 127.8, 85.7, 17.0, 16.1. TOF MALDI-HRMS: calcd ($[C_{19}H_{17}BN_2F_2I_2]^+$), m/z 575.9542, found, m/z 575.9528.

3.11. Synthesis of B-1. Compound **5** (28 mg, 0.03 mmol) and excess NIS (558 mg, 2.48 mmol) were dissolved in dry CH_2Cl_2 (25 mL). The mixture was stirred at 30 °C for 5 h. After completion of the reaction, the mixture was washed with saturated $Na_2S_2O_3{\cdot}5H_2O$ aqueous solution and was extracted with DCM. The organic layer was dried over anhydrous Na_2SO_4, and then the solvent was removed under reduced pressure. The residue was purified with column chromatography (silica gel, CH_2Cl_2) to give a red solid (34 mg, yield: 95%). Mp: >250 °C. ^{1}H NMR ($CDCl_3$, 400 MHz): δ 8.76−8.64 (m, 4H), 8.57 (s, 1H), 8.10 (dd, 2H, J_1 =8.0 Hz, J_2 = 20 Hz), 7.75 (d, 2H, J = 8.0 Hz), 7.49 (d, 2H, J = 8.0 Hz), 4.20−4.07 (m, 4H), 2.68 (d, 6H, J = 12.0 Hz), 1.98−1.95 (m, 2H), 1.43−1.31 (m, 16H), 1.26 (s, 6H), 0.98−0.88 (m, 12H). ^{13}C NMR (100 MHz, $CDCl_3$): δ 163.8, 163.5, 144.5, 140.1, 139.9, 136.1, 135.2, 134.9, 134.4, 134.4, 132.7, 131.4, 131.4, 130.1, 130.0, 129.5, 129.1, 128.5, 128.1, 127.6, 123.9, 123.3, 123.1, 122.8, 122.5, 86.2, 44.4, 38.0,

DOI: 10.1021/jo502899p
J. Org. Chem. 2015, 80, 3036−3049

30.8, 30.7, 28.7, 24.0, 23.1, 17.4, 16.2, 14.2, 10.7. TOF MALDI-HRMS: calcd ($[C_{59}H_{57}N_4O_4F_2BI_2]^-$), m/z 1188.2530; found, m/z 1188.2512.

3.12. Synthesis of B-2. The compound **6** (38 mg, 0.03 mmol) and NIS (558 mg, 2.48 mmol) were dissolved in dry CH_2Cl_2 (25 mL). The mixture was stirred at 30 °C for 12 h. After completion of the reaction, the mixture was washed with saturated $Na_2S_2O_3{\cdot}5H_2O$ aqueous solution and extracted with DCM. The organic layer was dried over anhydrous Na_2SO_4, and then the solvent was removed under reduced pressure. The residue was purified with column chromatography (silica gel, CH_2Cl_2) to give a red solid (34 mg, yield: 65%). Mp: >250 °C. ^{1}H NMR ($CDCl_3$, 500 MHz): δ 8.66 (s, 2H), 8.10 (dd, 4H, J_1 = 8.0 Hz, J_2 = 24 Hz), 7.82 (d, 4H, J = 8.0 Hz), 7.49 (d, 4H, J = 8.0 Hz), 4.21−4.09 (m, 4H), 2.68 (s, 12H), 1.98−1.93 (m, 2H), 1.45−1.33 (m, 16H), 1.26 (s, 12H), 0.97−0.88 (m, 12H). ^{13}C NMR (100 MHz, $CDCl_3$): δ 163.9, 163.6, 157.6, 144.0, 140.1, 135.8, 135.6, 134.7, 132.7, 131.3, 130.7, 130.6, 130.2, 129.5, 129.5, 128.2, 122.8, 122.7, 86.4, 44.7, 38.2, 31.0, 28.9, 24.3, 23.3, 16.3, 14.3, 10.9. TOF MALDI-HRMS: calcd ($[C_{78}H_{72}B_2N_6O_4F_4I_4]^-$), m/z 1762.1916, found, m/z 1762.1892.

3.13. Nanosecond Transient Absorption Spectra. The nanosecond transient absorption spectra were measured on an LP920 laser flash photolysis spectrometer (Edinburgh Instruments, U.K.) and recorded with a Tektronix TDS 3012B oscilloscope and a nanosecond pulsed laser (OpoletteTM 355II+UV nanosecond pulsed laser, typical pulse length 7 ns, pulse repetition 20 Hz, peak OPO energy 4 mJ, wavelength tunable in the range of 410−2200 nm; OPOTEK, USA). The lifetime values (by monitoring the decay trace of the transients) were obtained with LP900 software. All samples in flash photolysis experiments were deaerated with N_2 for ca. 15 min before measurement, and the gas flow was maintained during the measurements.

3.14. Cyclic Voltammetry. Cyclic voltammetry was performed using a CHI610D electrochemical workstation (Shanghai, People's Republic of China). Cyclic voltammograms were recorded at scan rates of 0.05 V/s. The electrolytic cell used was a three-electrode cell. Electrochemical measurements were performed at room temperature using 0.1 M tetrabutylammonium hexafluorophosphate ($Bu_4N[PF_6]$) as supporting electrolyte, after purging with N_2. The working electrode was a glassy-carbon electrode, and the counter electrode was a platinum electrode. A nonaqueous $Ag/AgNO_3$ (0.1 M in acetonitrile) reference electrode was contained in a separate compartment connected to the solution via a semipermeable membrane. Dichloromethane was used as the solvent. Ferrocene was added as the an internal reference.

■ ASSOCIATED CONTENT

Supporting Information

Text, figures, and tables giving general experimental methods, molecular structure characterization, and additional spectra. This material is available free of charge via the Internet at http://pubs.acs.org.

■ AUTHOR INFORMATION

Corresponding Authors

*E-mail for J.Z.: zhaojzh@dlut.edu.cn.

*E-mail for M.H.: hayvali@science.ankara.edu.tr.

Notes

The authors declare no competing financial interest.

■ ACKNOWLEDGMENTS

We thank the NSFC (21073028, 21273028, 51202207, 21473020 and 21421005), the Royal Society (U.K.) and NSFC (China-UK Cost-Share Science Networks, 21011130154), Science Foundation Ireland (SFI ETS Walton Program 11/W.1/E2061), Program for Changjiang Scholars and Innovative Research Team in University [IRT_13R06], State Key Laboratory of Fine Chemicals (KF1203), the Fundamental Research Funds for the Central Universities (DUT14ZD226), and Dalian University of Technology (DUT2013TB07) for financial support.

■ REFERENCES

(1) McDonnell, S. O.; Hall, M. J.; Allen, L. T.; Byrne, A.; Gallagher, W. M.; O'Shea, D. F. *J. Am. Chem. Soc.* **2005**, *127*, 16360−16361.

(2) Yukruk, F.; Dogan, A. L.; Canpinar, H.; Guc, D.; Akkaya, E. U. *Org. Lett.* **2005**, *7*, 2885−2887.

(3) (a) Awuah, S. G.; You, Y. *RSC Adv.* **2012**, *2*, 11169−11183. (b) Fan, J.; Hu, M.; Zhan, P.; Peng, X. *Chem. Soc. Rev.* **2013**, *42*, 29−43.

(4) Kamkaew, A.; Lim, S. H.; Lee, H. B.; Kiew, L. V.; Chung, L. Y.; Burgess, K. *Chem. Soc. Rev.* **2013**, *42*, 77−88.

(5) Cakmak, Y.; Kolemen, S.; Duman, S.; Dede, Y.; Dolen, Y.; Kilic, B.; Kostereli, Z.; Yildirim, L. T.; Dogan, A. L.; Guc, D.; et al. *Angew. Chem., Int. Ed.* **2011**, *50*, 11937−11941.

(6) Zhao, J.; Wu, W.; Sun, J.; Guo, S. *Chem. Soc. Rev.* **2013**, *42*, 5323−5351.

(7) (a) Lazarides, T.; Charalambidis, G.; Vuillamy, A.; Reglier, M.; Klontzas, E.; Froudakis, G.; Kuhri, S.; Guldi, D. M.; Coutsolelos, A. G. *Inorg. Chem.* **2011**, *50*, 8926−8936. (b) Li, Y.; Liu, R.; Badaeva, E.; Kilina, S.; Sun, W. *J. Phys. Chem. C* **2013**, *117*, 5908−5918. (c) Liu, R.; Li, Y.; Chang, J.; Waclawik, E. R.; Sun, W. *Inorg. Chem.* **2014**, *53*, 9516−9530. (d) Liu, R.; Dandu, N.; Chen, J.; Li, Y.; Li, Z.; Liu, S.; Wang, C.; Kilina, S.; Köhler, B.; Sun, W. *J. Phys. Chem. C* **2014**, *118*, 23233−23246.

(8) (a) Bartelmess, J.; Francis, A. J.; El Roz, K. A.; Castellano, F. N.; Weare, W. W.; Sommer, R. D. *Inorg. Chem.* **2014**, *53*, 4527−4534. (b) Kim, S.; Lee, G. Y.; Baeg, J.-O.; Kim, Y.; Kim, S.-J.; Kim, J. *J. Phys. Chem. C* **2014**, *118*, 25844−25852. (c) Kim, J. A.; Kim, S.; Lee, J.; Baeg, J.-O.; Kim, J. *Inorg. Chem.* **2012**, *51*, 8057−8063.

(9) Shi, L.; Xia, W. *Chem. Soc. Rev.* **2012**, *41*, 7687−7697.

(10) Lalevee, J.; Peter, M.; Dumur, F.; Gigmes, D.; Blanchard, N.; Tehfe, M.; Morlet-Savary, F.; Fouassier, J. P. *Chem.—Eur. J.* **2011**, *17*, 15027−15031.

(11) Singh-Rachford, T. N.; Castellano, F. N. *Coord. Chem. Rev.* **2010**, *254*, 2560−2573.

(12) Monguzzi, A.; Tubino, R.; Hoseinkhani, S.; Campione, M.; Meinardi, F. *Phys. Chem. Chem. Phys.* **2012**, *14*, 4322−4332.

(13) Simon, Y. C.; Weder, C. *J. Mater. Chem.* **2012**, *22*, 20817−20830.

(14) Zhao, J.; Ji, S.; Guo, H. *RSC Adv.* **2011**, *1*, 937−950.

(15) (a) Ceroni, P. *Chem. Eur. J.* **2011**, *17*, 9560−9564. (b) Wang, B.; Sun, B.; Wang, X.; Ye, C.; Ding, P.; Liang, Z.; Chen, Z.; Tao, X.; Wu, L. *J. Phys. Chem. C* **2014**, *118*, 1417−1425.

(16) Papkovsky, D. B.; O'Riordan, T. C. *J. Fluoresc.* **2005**, *15*, 569−584.

(17) Lim, J. M.; Yoon, Z. S.; Shin, J.-Y.; Kim, K. S.; Yoon, M.; Kim, D. *Chem. Commun.* **2009**, *3*, 261−273.

(18) Carvalho, C. M. B.; Brocksom, T. J.; Thiago de Oliveira, K. *Chem. Soc. Rev.* **2013**, *42*, 3302−3317.

(19) Schmitt, F.; Freudenreich, J.; Barry, N. P. E.; Juillerat-Jeanneret, L.; Suss-Fink, G.; Therrien, B. *J. Am. Chem. Soc.* **2012**, *134*, 754−757.

(20) Liu, Q.; Li, Y.; Zhang, H.; Chen, B.; Tung, C.; Wu, L. *Chem. Eur. J.* **2012**, *18*, 620−627.

(21) Specht, D. P.; Martic, P. A.; Farid, S. *Tetrahedron* **1982**, *38*, 1203−1211.

(22) Borak, J. B.; Falvey, D. E. *Photochem. Photobiol. Sci.* **2010**, *9*, 854−860.

(23) You, Y.; Nam, W. *Chem. Soc. Rev.* **2012**, *41*, 7061−7084.

(24) (a) Duman, S.; Cakmak, Y.; Kolemen, S.; Akkaya, E. U.; Dede, Y. *J. Org. Chem.* **2012**, *77*, 4516−4527. (b) Yang, Y.; Guo, Q.; Chen, H.; Zhou, Z.; Guo, Z.; Shen, Z. *Chem. Commun.* **2013**, *49*, 3940−3942.

(25) Topel, S. D.; Cin, G. T.; Akkaya, E. U. *Chem. Commun.* **2014**, *50*, 8896−8899.

(26) Wu, W.; Zhao, J.; Guo, H.; Sun, J.; Ji, S.; Wang, Z. *Chem. Eur. J.* **2012**, *18*, 1961−1968.

(27) (a) Borisov, S. M.; Saf, R.; Fischer, R.; Klimant, I. *Inorg. Chem.* **2013**, *52*, 1206−1216. (b) To, W.-P.; Chan, K. T.; Tong, G. S. M.; Ma, C.; Kwok, W.-M.; Guan, X.; Low, K.-H.; Che, C.-M. *Angew. Chem., Int. Ed.* **2013**, *52*, 6648−6652.

(28) Peng, J.; Jiang, X.; Guo, X.; Zhao, D.; Ma, Y. *Chem. Commun.* **2014**, *50*, 7828−7830.

DOI: 10.1021/jo502899p
J. Org. Chem. 2015, 80, 3036−3049

(29) Sun, J.; Zhong, F.; Yi, X.; Zhao, J. *Inorg. Chem.* **2013**, *52*, 6299−6310.
(30) Erbas-Cakmak, S.; Bozdemir, O. A.; Cakmak, Y.; Akkaya, E. U. *Chem. Sci.* **2013**, *4*, 858−862.
(31) Altan Bozdemir, O.; Erbas-Cakmak, S.; Ekiz, O. O.; Dana, A.; Akkaya, E. U. *Angew. Chem., Int. Ed.* **2011**, *50*, 10907−10912.
(32) El-Khouly, M. E.; Amin, A. N.; Zandler, M. E.; Fukuzumi, S.; D'Souza, F. *Chem. Eur. J.* **2012**, *18*, 5239−5247.
(33) Bura, T.; Nastasi, F.; Puntoriero, F.; Campagna, S.; Ziessel, R. *Chem. Eur. J.* **2013**, *19*, 8900−8912.
(34) Serin, J. M.; Brousmiche, D. W.; Frechet, J. M. J. *J. Am. Chem. Soc.* **2002**, *124*, 11848−11849.
(35) Zhang, C.; Zhao, J.; Wu, S.; Wang, Z.; Wu, W.; Ma, J.; Guo, S.; Huang, L. *J. Am. Chem. Soc.* **2013**, *135*, 10566−10578.
(36) (a) Guo, S.; Ma, L.; Zhao, J.; Kuecuekoez, B.; Karatay, A.; Hayvali, M.; Yaglioglu, H. G.; Elmali, A. *Chem. Sci.* **2014**, *5*, 489−500. (b) Ma, J.; Yuan, Xi.; Kucukoz, B.; Li, S.; Zhang, C.; Majumdar, P.; Karatay, A.; Li, X.; Yaglioglu, H. G.; Elmali, A.; Zhao, J.; Hayvali, M. *J. Mater. Chem. C* **2014**, *2*, 3900−3913.
(37) Erbas-Cakmak, S.; Akkaya, E. U. *Angew. Chem., Int. Ed.* **2013**, *52*, 11364−11368.
(38) Hofmann, C. C.; Lindner, S. M.; Ruppert, M.; Hirsch, A.; Haque, S. A.; Thelakkat, M.; Köhler, J. *J. Phys. Chem. B* **2010**, *114*, 9148−9156.
(39) Yarnell, J. E.; Deaton, J. C.; McCusker, C. E.; Castellano, F. N. *Inorg. Chem.* **2011**, *50*, 7820−7830.
(40) Whited, M. T.; Djurovich, P. I.; Roberts, S. T.; Durrell, A. C.; Schlenker, C. W.; Bradforth, S. E.; Thompson, M. E. *J. Am. Chem. Soc.* **2011**, *133*, 88−96.
(41) Lazarides, T.; McCormick, T. M.; Wilson, K. C.; Lee, S.; McCamant, D. W.; Eisenberg, R. *J. Am. Chem. Soc.* **2011**, *133*, 350−364.
(42) Zhang, J.; Fischer, M. K. R.; Bauerle, P.; Goodson, T. *J. Phys. Chem. B* **2013**, *117*, 4204−4215.
(43) Costa, R. D.; Cespedes-Guirao, F. J.; Bolink, H. J.; Fernandez-Lazaro, F.; Sastre-Santos, A.; Orti, E.; Gierschner, J. *J. Phys. Chem. C* **2009**, *113*, 19292−19297.
(44) Ziessel, R.; Harriman, A. *Chem. Commun.* **2011**, *47*, 611−631.
(45) Loudet, A.; Burgess, K. *Chem. Rev.* **2007**, *107*, 4891−4932.
(46) Qian, H.; Wang, Z.; Yue, W.; Zhu, D. *J. Am. Chem. Soc.* **2007**, *129*, 10664−10665.
(47) Neuteboom, E. E.; Meskers, S. C. J.; Beckers, E. H. A.; Chopin, S.; Janssen, R. A. J. *J. Phys. Chem. A* **2006**, *110*, 12363−12371.
(48) Lin, M.; Jimenez, A. J.; Burschka, C.; Würthner, F. *Chem. Commun.* **2012**, *48*, 12050−12052.
(49) Ventura, B.; Langhals, H.; Boeck, B.; Flamigni, L. *Chem. Commun.* **2012**, *48*, 4226−4228.
(50) Sunahara, H.; Urano, Y.; Kojima, H.; Nagano, T. *J. Am. Chem. Soc.* **2007**, *129*, 5597−5604.
(51) Wu, W.; Guo, H.; Wu, W.; Ji, S.; Zhao, J. *J. Org. Chem.* **2011**, *76*, 7056−7064.
(52) Bozdemir, O. A.; Yilmaz, M. D.; Buyukcakir, O.; Siemiarczuk, A.; Tutas, M.; Akkaya, E. U. *New J. Chem.* **2010**, *34*, 151−155.
(53) William, E.; Kamat, P. V. *J. Phys. Chem.* **1987**, *91*, 6373−80.
(54) Rachford, A. A.; Ziessel, R.; Bura, T.; Retailleau, P.; Castellano, F. N. *Inorg. Chem.* **2010**, *49*, 3730−3736.
(55) Zhang, L.; Chen, B.; Wu, L.; Tung, C.; Cao, H.; Tanimoto, Y. *Chem. Eur. J.* **2003**, *9*, 2763−2769.
(56) Feng, K.; Yu, M.; Wang, S.; Wang, G.; Tung, C.; Wu, L. *ChemPhysChem* **2013**, *14*, 198−203.
(57) Benniston, A. C.; Copley, G. *Phys. Chem. Chem. Phys.* **2009**, *11*, 4124−4131.
(58) Ulrich, G.; Ziessel, R.; Harriman, A. *Angew. Chem, Int. Ed.* **2008**, *47*, 1184−1201.
(59) Apperloo, J. J.; Martineau, C.; van Hal, P. A.; Roncali, J.; Janssen, R. A. J. *J. Phys. Chem. A* **2002**, *106*, 21−31.
(60) Zhang, X.; Xiao, Y.; Qian, X. *Org. Lett.* **2008**, *10*, 29−32.
(61) Sabatini, R. P.; McCormick, T. M.; Lazarides, T.; Wilson, K. C.; Eisenberg, R.; McCamant, D. W. *J. Phys. Chem. Lett.* **2011**, *2*, 223−227.
(62) Hippius, C.; Van Stokkum, I. H. M.; Zangrando, E.; Williams, R. M.; Würthner, F. *J. Phys. Chem. C* **2007**, *111*, 13988−13996.
(63) Wu, Y.; Zhen, Y.; Wang, Z.; Fu, H. *J. Phys. Chem. A* **2013**, *117*, 1712−1720.
(64) (a) Ziessel, R.; Allen, B. D.; Rewinska, D. B.; Harriman, A. *Chem. Eur. J.* **2009**, *15*, 7382−7393. (b) Zhang, X.-F.; Wang, J. *J. Phys. Chem. A* **2011**, *115*, 8597−8603.
(65) Liu, Y.; Zhao, J. *Chem. Commun.* **2012**, *48*, 3751−3753.
(66) Sun, J.; Zhong, F.; Zhao, J. *Dalton Trans.* **2013**, *42*, 9595−9605.
(67) Zhang, X.-F.; Yang, X. *J. Phys. Chem. B* **2013**, *117*, 5533−5539.
(68) Rachford, A. A.; Goeb, S.; Castellano, F. N. *J. Am. Chem. Soc.* **2008**, *130*, 2766−2767.
(69) Llewellyn, B. A.; Slater, A. G.; Goretzki, G.; Easun, T. L.; Sun, X.; Davies, E. S.; Argent, S. P.; Lewis, W.; Beeby, A.; George, M. W.; et al. *Dalton Trans.* **2014**, *43*, 85−94.
(70) Zhang, R.; Wu, Y.; Wang, Z.; Xue, W.; Fu, H.; Yao, J. *J. Phys. Chem. C* **2009**, *113*, 2594−2602.
(71) Kircher, T.; Lohmannsroben, H. *Phys. Chem. Chem. Phys.* **1999**, *1*, 3987−3992.
(72) El-Khouly, M. E.; Fukuzumi, S. *J. Porphyrins Phthalocyanines* **2011**, *15*, 111−117.
(73) Ahrens, M. J.; Sinks, L. E.; Rybtchinski, B.; Liu, W.; Jones, B. A.; Giaimo, J. M.; Gusev, A. V.; Goshe, A. J.; Tiede, D. M.; Wasielewski, M. R. *J. Am. Chem. Soc.* **2004**, *126*, 8284−8294.
(74) Flors, C.; Oesterling, I.; Schnitzler, T.; Fron, E.; Schweitzer, G.; Sliwa, M.; Herrmann, A.; Van der Auweraer, M.; De Schryver, F. C.; Muellen, K.; et al. *J. Phys. Chem. C* **2007**, *111*, 4861−4870.
(75) Giaimo, J. M.; Lockard, J. V.; Sinks, L. E.; Scott, A. M.; Wilson, T. M.; Wasielewski, M. R. *J. Phys. Chem. A* **2008**, *112*, 2322−2330.
(76) Harriman, A.; Alamiry, M. A. H.; Hagon, J. P.; Hablot, D.; Ziessel, R. *Angew. Chem., Int. Ed.* **2013**, *52*, 6611−6615.
(77) Lakowicz, J. R. *Principles of Fluorescence Spectroscopy*, 2nd ed.; Kluwer Academic: New York, 1999.
(78) Valeur, B. *Molecular Fluorescence: Principles and Applications*; Wiley-VCH: Weinheim, Germany, 2001.
(79) Turro, N. J.; Ramamurthy, V.; Scaiano, J. C. *Principles of Molecular Photochemistry: An Introduction*; University Science Books: Sausalito, CA, 2009.

DOI: 10.1021/jo502899p
J. Org. Chem. 2015, 80, 3036−3049